Generation of Reproducible Model Freshwater Particulate Matter Analogues to Study the Interaction with Particulate Contaminants.

Helene Walch [a, 1], *Antonia Praetorius* [a, b], *Frank von der Kammer* [a, *], *Thilo Hofmann* [a, *]

[a] Department of Environmental Geosciences, Centre for Microbiology and Environmental Systems Science, University of Vienna, Althanstraße 14, UZA II, 1090 Vienna, Austria

[b] Department of Ecosystem & Landscape Dynamics, Institute for Biodiversity and Ecosystem Dynamics, University of Amsterdam, Science Park 904, 1098 XH Amsterdam, The Netherlands

h.walch@gmx.at, a.praetorius@uva.nl, frank.kammer@univie.ac.at, thilo.hofmann@univie.ac.at

[*] Corresponding authors: Thilo Hofmann and Frank von der Kammer

This is a non-peer reviewed preprint submitted to EarthArXiv. The manuscript has been submitted to *Water Research* for peer review.

---

[1] Present Address: Studies & Consulting, Laboratories, Environment Agency Austria, Spittelauer Lände 5, 1090 Vienna, Austria, helene.walch@umweltbundesamt.at

Abstract: Aquatic fate models and risk assessment require experimental information on the potential of contaminants to interact with riverine suspended particulate matter (SPM). While for dissolved contaminants partition or sorption coefficients are used, the underlying assumption of chemical equilibrium is invalid for particulate contaminants, such as engineered nanomaterials, incidental nanoparticles, micro- or nanoplastics. Their interactions with SPM are governed by physicochemical forces between contaminant-particle and SPM surfaces. The availability of a standard SPM material is thus highly relevant for the development of reproducible test systems to evaluate the fate of particulate contaminants in aquatic systems. Finding suitable SPM analogues, however, is challenging considering the complex composition of natural SPM, which features floc-like structures comprising minerals and organic components from the molecular to the microorganism level. Complex composition comes with a heterogeneity in physicochemical surface properties, that cannot be neglected. We developed a procedure to generate SPM analogue flocs from components selected to represent the most abundant and crucial constituents of natural riverine SPM, and the process-relevant SPM surface characteristics regarding interactions with particulate contaminants. Four components, i.e., illite, hematite, quartz and tryptophan, combined at environmentally realistic mass-ratios, were associated to complex flocs. Flocculation was reproducible regarding floc size and fractal dimension, and multiple tests on floc resilience towards physical impacts (agitation, sedimentation-storage-resuspension, dilution) and hydrochemical changes (pH, electrolytes, dissolved organic matter concentration) confirmed their robustness. These reproducible, ready-to-use SPM analogue flocs will strongly support future research on emerging particulate contaminants.

Keywords: suspended particulate matter, environmental risk assessment, fate, heteroagglomeration, nanoparticles, microplastics

Abbreviations: SPM: suspended particulate matter; NOM: natural organic matter; EPS: extracellular polymeric substances; FeOx: iron oxides and (oxy)hydroxide minerals; SR-NOM: Suwannee River natural organic matter; TOC: total organic carbon; SEM: scanning electron microscopy; $d_{V0.5}$: volume-based median diameter, D_f: volume fractal dimension; mode d_V: volume-based diameter; SPMzero: SPM analogues generated without electrolyte or SR-NOM addition; RSD: relative standard deviation; ave: average; sd: standard deviation

1. Introduction

River-systems are among the major contaminant-receiving waters and constitute potential long-range environmental transport routes. Contaminant transport and fate depend on their interactions with natural materials, which are present in all forms – from truly dissolved, through colloidal and suspended particulate matter, to bed load and bottom sediments. Within this continuum of matter, a crucial role can be attributed to suspended particulate matter (SPM) because (1) SPM is in constant exchange with all other phases, through adsorption/desorption, attachment/detachment, (de–)agglomeration, flocculation/rupture and sedimentation/resuspension, (2) SPM is mobile and links the pelagic and benthic zones (by sedimentation and resuspension), rivers to lakes and oceans (by advective transport) and terrestrial to aquatic environments (via erosion and runoff, or flooding), and (3) SPM provides habitat and feed to aquatic organisms (Walch et al., 2022). The affinity of contaminants for SPM depends on both their respective properties, and governs their transport behavior, bioavailability, uptake, and fate (Geitner et al., 2016; Hofmann and von der Kammer, 2009; Schulze et al., 2015).

A quantification of contaminant-SPM interactions is needed for exposure assessment in the framework of environmental risk assessment. For dissolved contaminants, classical solid/liquid partition coefficients (K_d) can be employed to describe the affinity of a contaminant for water *versus* solid phases. Over the past decades, however, particulate contaminants, such as engineered nanomaterials, micro- or nanoplastics, received increased attention, and chemical legislation (e.g., REACH, TSCA) requiring environmental risk assessment is adapted to cover these contaminants. This has triggered scientific debate about suitable fate descriptors for particulate contaminants (Dale et al., 2015; Praetorius et al., 2014b; Svendsen et al., 2020; Westerhoff and Nowack, 2013). Praetorius et al. (2014) emphasized that partition coefficients cannot be employed for particulate contaminants, as the underlying thermodynamic equilibrium assumption is only applicable for dissolved substances. Consequently, calls for harmonized testing protocols specific to particulate contaminants (Baun et al., 2017; Stone et al., 2010) can only be responded to while accounting for the process-relevant interaction mechanisms.

Interactions between particulate contaminants and SPM (i.e., heteroagglomeration) are kinetically driven (Praetorius et al., 2014b) and governed by short-range physicochemical surface interactions. As depicted in Figure 1, interaction forces (mainly electrostatic, hydrophobic, and van der Waals forces, or NOM-interactions) arise from the interplay of intrinsic material properties of both, particulate contaminants and SPM, and hydrochemical conditions (mainly pH, electrolytes, and NOM: natural organic matter) (Elimelech et al., 1995; Gregory, 2005). The effects of intrinsic and extrinsic factors cannot be easily disentangled, especially regarding more complex multi-component systems (Praetorius et al., 2020). Consequently, protocols to test particulate contaminants' affinity for SPM require accounting for both, the process-relevant physicochemical surface properties of natural SPM and the relevant hydrochemical conditions.

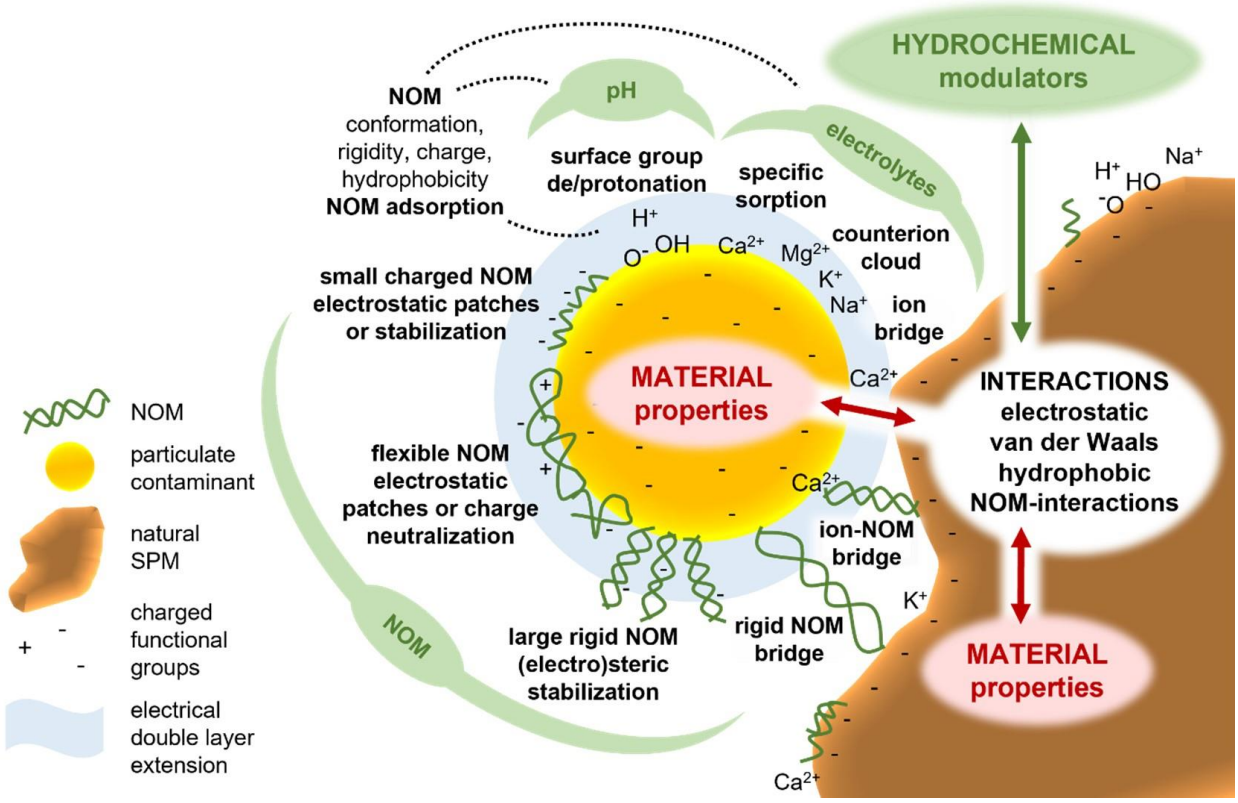

Figure 1. Material-dependent interaction forces between SPM and particulate contaminants as modulated by hydrochemistry.

Freshwater hydrochemical conditions were recently operationalized within the OECD test guideline No. 318 *Dispersion stability of nanomaterials in simulated environmental media* (OECD, 2017) and the rationale beyond the selected hydrochemical test parameter ranges (Abdolahpur Monikh et al., 2018) is directly applicable to heteroagglomeration. Hence, the selection of suitable counterparts for heteroagglomeration, ideally SPM analogues which represent the agglomeration-relevant natural properties, remains one major gap to fill (Praetorius et al., 2020). Achieving this task is hampered by the complexity and spatiotemporal variability of natural riverine SPM (Walch et al., 2022). SPM is operationally defined and comprises any materials that

do not sediment under the given hydrodynamic and hydrochemical conditions and get retained by 0.45 or 0.22 µm filtration membranes (Eisma, 1993). SPM typically exhibits agglomerate or floc-like structures, integrating minerals and organic components (from molecules, via detritus up to microorganisms) of alloch- and autochthonous origins (Droppo, 2001; Henning et al., 2001; Zimmermann-Timm, 2002), with each component contributing distinct physicochemical surface properties to a floc (Walch et al., 2022).

Most heteroagglomeration studies either employed simple mineral SPM surrogates (e.g., Gallego-Urrea et al., 2016; Labille et al., 2015; Oriekhova and Stoll, 2018; Praetorius et al., 2014a; Yu et al., 2021; Zhou et al., 2012) or natural water samples (e.g., Quik *et al.*, 2014; Velzeboer *et al.*, 2014; Adam *et al.*, 2016; Li *et al.*, 2019; Surette and Nason, 2019), but neither meet the need for environmentally relevant and yet standardizable test conditions. Simple minerals do not reflect the complexity and heterogeneity of natural SPM, while natural samples do not allow for reproducibility, since the properties of natural SPM are specific to a certain sampling location and time. So far, the only publication reporting near-natural SPM is Slomberg et al. (2016), who tried to assemble SPM analogues based on the mineralogical composition of SPM from the Rhône catchment. However, they included only major (negatively charged) mineral fractions, neglecting minor but functionally important components such as positively charged oxide and (oxy)hydroxide minerals, or microbial extracellular polymeric substances (EPS) (Walch et al., 2022).

Standardization requires simplification, but a valid model test system needs to cover the most relevant factors which control the process under observation. Hence, we took a conceptual approach to select key components for the generation of complex SPM analogue flocs, developed a simple protocol for their association, and finally evaluated their robustness and handling in the laboratory. The detailed rationale beyond component selection is given in the conceptual

framework (supporting information S1). Briefly, we aimed at tailoring SPM analogues that represent those characteristics of natural riverine SPM which are most relevant for heteroagglomeration. Analogues should reflect the complex composition/structure of natural SPM, as well as its heterogeneity in physicochemical surface properties, while comprising only few components to allow for reproducible generation. Our component selection is based on an extensive literature review (Walch et al., 2022), looking at the mineralogical and organic composition of natural riverine SPM and crucial components governing the dynamics of SPM formation. Selected minerals comprise illite, quartz, and hematite; and the amino acid tryptophan was chosen as a proxy for microbial EPS (based on screening tests S2). Illite and quartz are representatives for the most abundant mineral constituents of natural riverine SPM, and hematite for minor but functionally important iron oxide and (oxy)hydroxide minerals (FeOx). Similarly, microbial EPS are mostly less abundant in SPM than refractory humic-like substances, but due to their heterogeneous properties, EPS are considered more relevant for flocculation. Being combined in realistic mass-ratios, the selected components not only reflect the composition of natural SPM, but also add to an increased heterogeneity in physicochemical surface properties, which is probably the most relevant feature of natural SPM when it comes to interactions with particulate contaminants.

The aim of this study was to develop and test reproducible SPM analogue flocs. We show that, using illite, quartz, hematite, and tryptophan in realistic mass-ratios, it is possible to generate complex SPM analogues, which are consistent regarding floc size and fractal dimension, and exhibit the desired robustness towards physical impacts and hydrochemical changes to allow proper handling in experimental setups.

2. Materials and Methods

2.1. Hydrochemical Background

Following OECD test guideline No. 318 (OECD, 2017), hydrochemical test conditions comprised a pH range of 5-8.5, Suwannee River NOM (SR-NOM) at 0.1-10 ppmC and 0.1-10 mM $CaCl_2$ and $MgSO_4$ at a molar ratio of Ca:Mg 4:1 (hereafter just referred to as electrolytes). $CaCl_2$ was used, instead of $CaNO_3$ suggested by the guideline's *alternative medium*, because Cl^- is more abundant in river waters than NO_3^- (Salminen et al., 2005). SR-NOM stock was prepared according to the guideline: SR-NOM powder (2R101N, International Humic Substances Society) was dissolved in ultrapure water at pH 8 while agitating (> 16 h). After readjusting the pH and filtering the solution (sterile 0.2 µm PES bottle-top filters, Nalgene), the non-purgeable organic carbon concentration was determined with a total organic carbon (TOC) analyzer (TOC-L CPH/CPN, Shimadzu), and with 40 ± 1.5 $\%_{wt}$ was close to the expected values of 42.6 $\%_{wt}$ (Perdue, 2012) or 46.2 $\%_{wt}$ (IHSS, 2020a). Electrolyte solutions were prepared from calcium chloride dihydrate (≥ 99 %, Sigma Aldrich) and magnesium sulfate heptahydrate (≥ 99.5 %, EMSURE, Merck) at 800 or 80 and 200 or 20 mM, respectively, to receive a 4:1 Ca:Mg molar ratio in 1:1 mixtures. Intended pH values were adjusted with 0.1 M NaOH or HCl and monitored during measurements. Only at pH 8.5 the value dropped and had to be readjusted/maintained by constant NaOH additions during measurements (<0.1% of the total sample volume).

2.2. SPM Analogue Components

Details on illite and hematite stock preparation are given in the supporting information (S3-A and S3-B). Briefly, illite rock chips (IMt-2, Silver Hill, MT, USA, Clay Minerals Society), were

milled, dispersed, Na-exchanged and washed in repeated centrifugation-resuspension cycles, before narrowing the size distribution by differential centrifugation. Hematite was prepared by forced hydrolysis according to Wang et al. (2008). Quartz powder (SiO_2 0.5 µm spheres, Alfa Aesar) was dispersed in ultrapure water (weigh-in 1.5 g L^{-1}) using an ultrasonic probe (40 min, 40 W, TT13 tip, Sonoplus 3200, Bandelin). Dispersion efficacy was confirmed by checking hydrodynamic diameters (Zetasizer Nano ZS, Malvern). Characterization of mineral suspensions comprised hydrodynamic diameters, zeta potentials, polydispersity indices, isoelectric point determination in different hydrochemical backgrounds, and scanning electron microscopy (SEM) imaging, as reported in S3-C. L-Tryptophan solution was prepared at a carbon concentration of 2 g L^{-1} based on the carbon mass fraction in tryptophan (64.7 %), dissolving the powder (≥ 98 %, Sigma Aldrich) in ultrapure water by overnight shaking. Carbon recoveries, determined on a TOC analyzer (see 2.1.), were 98 ± 4 %. All stocks were stored in the dark at 4°C. The stability of mineral stocks was evaluated checking hydrodynamic diameters and zeta potentials (Zetasizer Nano ZS, Malvern) before use. Hematite suspensions were stable for 6 months (Figure S3-1), illite and quartz can be stored for at least one year, with quartz requiring 15-20 min ultrasonic probe sonication before use after resting for more than a few days. Organic stocks were replaced every two months.

2.3. SPM Analogue Generation

For SPM analogue flocculation and characterization, a batch setup consisting of two stirred batch reactors connected to a laser diffractometer (Mastersizer 2000, Malvern) was designed, where the sample was passed through the measurement cell in "freefall" (~ 6 mL s^{-1}) to avoid any change in floc size or fractal dimension, with a peristaltic pump closing the circuit between the two batch

reactors (S4-A). SPM analogue composition (Table 1) was based on typical riverine SPM compositions (see S1 and (Walch et al., 2022)) and screening tests (S2) and refined within the Mastersizer setup (S4-B). Starting from quartz and illite in ultrapure water at pH 5 (to maintain the positive surface charge of hematite upon addition), dilutions of hematite, tryptophan, electrolyte and SR-NOM stocks were quickly added (<15 s) in this sequence to both stirred batches simultaneously, establishing the SPM component concentrations given in Table 1, as well as the targeted hydrochemical background concentrations in a final volume of 800 mL for each batch (for details see S4-C).

Table 1. SPM analogue component fractions and final concentrations

		Mass fractions [$\%_{wt}$]	**Conc. [mg L^{-1}]**
Illite:Quartz Ratio 55:45	Quartz	41.85	18.83
	Illite	51.15	23.02
Hematite		7	3.15
Total mineral		*100*	*45*
Tryptophan (C-based)		+5 % to minerals	2.25

Two procedures to generate SPM analogues were followed. (1) *Association procedure*: preparation directly in the two stirred batches connected to the Mastersizer, where circulation through the system and measurement of the sample were started right before the addition of hematite, tryptophan, electrolytes and SR-NOM, which allowed investigating the flocculation process. (2) *Shaker equilibration*: components were added into two magnetically stirred bottles (1 L centrifuge bottles, Heraeus) and then left on an overhead shaker for 1-24 h (16 rpm, Reax 20, Heidolph), before introducing the suspension into the Mastersizer setup for characterization.

2.4. SPM Analogue Protocol Validation

Hydrochemical conditions employed for protocol validation were 0.1 mM electrolytes at pH 5, without SR-NOM addition (for reasoning see S5-A). The *association procedure* was repeated 4 times using the same component stocks for within-batch reproducibility, and 3 times employing different component-stock batches for between-batches reproducibility. The *shaker equilibration* was validated only within-batch (4 replicates). To test storability, SPM was prepared by *shaker equilibration* (shaken for 1 h) and stored in the dark fridge at 4°C. Three batches were repeatedly resuspended at increasing time intervals (1 h, 1, 4, 8, 20 and 48 d), by three different means: overhead shaking (1 h, 16 rpm, Reax 20, Heidolph), ultrasonic bath sonication (20 min) and ultrasonic probe sonication (10 min, 40 W, TT13 tip, Sonoplus 3200, Bandelin) applied to each storage bottle containing 800 mL. Four additional parallel batches were resuspended by overhead shaking after 0, 5, 9 and 15 days of storage, respectively, to investigate storability without interim resuspension. Robustness towards changes in SPM concentration and stirring speed was tested by halving the concentration (from 45 to 22.5 ppm) and by varying the stirring speed between 50, 100 and 150 rpm, both, during SPM association, and after storage and resuspension.

SPM analogue reproducibility, storability and robustness were evaluated regarding stability and resilience of floc size and fractal dimension by means of laser diffractometry (Mastersizer 2000, Malvern). Volume-based median diameters ($d_{V0.5}$) and volume fractal dimensions (D_f) were recorded and plotted in a time-resolved manner. Volume-based size distributions and mode diameters (mode d_V) were employed to compare samples at a specific time point. Details are given in S5-B. Additionally, SPM analogue floc morphology was investigated by SEM imaging, as described in S3-C.

2.5. SPM Analogues in Changing Hydrochemistry.

The formation of SPM analogues in varying hydrochemical backgrounds was evaluated regarding floc size and fractal dimension in the Mastersizer setup after overnight *shaker equilibration*. Electrolyte (0.1, 1, 10 mM) and SR-NOM concentrations (0, 0.1, 1, 10 ppmC) were varied at pH 5, and zeta potentials were measured according to S3-C. The impact of pH (values 5, 7, 8.5) was investigated in batches prepared at 0.1 mM electrolytes without any SR-NOM, and at 10 mM with 1 ppmC SR-NOM. Adjustments of pH were done during SPM preparation, before overnight shaking, and continuously during measurement.

To evaluate whether flocs keep their integrity when hydrochemistry is changed after floc formation, and may be transferred into different hydrochemistries, SPM was generated at pH 5 without any electrolytes or SR-NOM added (SPMzero). After association, the hydrochemistry was adjusted by adding diluted electrolyte and SR-NOM stocks to reach a hydrochemical background of 0.1 mM and 1 ppmC, while halving the SPM concentration to 22.5 ppm.

3. Results and Discussion

3.1. Complex Near-Natural SPM Analogue Flocs Can be Reproducibly Prepared.

Flocs formed within minutes with diameters consistently around 7 µm and fractal dimensions slightly above 2.5. Signals in the size range of the individual components were not recorded by the Mastersizer 2000. The individual component preparations were highly consistent (Table S3-1), meeting the criteria to allow a reproducible SPM analogue generation, which was confirmed regarding floc size and fractal dimension, whether the same (Figure S6-1) or different component

batches (Figure 2) were employed. After an initial floc association phase, the diameter and fractal dimension reached an interim plateau. Size distributions were stable during that time, narrow and consistent between replicates (Figure 2 b, Figure S6-1 b). The relative standard deviations (RSDs) of the volume-based mode diameters (mode d_V) compared after 1 h were 4.8 % (mode d_V = 7.3 µm, n = 4) and 6.7 % (mode d_V = 7.9 µm, n = 3), for within-batch and between-batches replicates (see 2.4.) respectively. The size of the flocs falls within the range of natural riverine floc sizes covering < 1 to 1000 µm (Zimmermann-Timm, 2002), with typical values from few µm up to (few) hundred µm (Guo and He, 2011; Lartiges et al., 2001; Woodward and Walling, 2007). Fractal dimensions exhibited values within the predetermined range for shear flow (i.e., ≥ 2.4) (Conchuir et al., 2014), with RSDs of 0.9 % (D_f = 2.56, n = 4) within-batch, and 5.1 % (D_f = 2.7, n = 3) between batches.

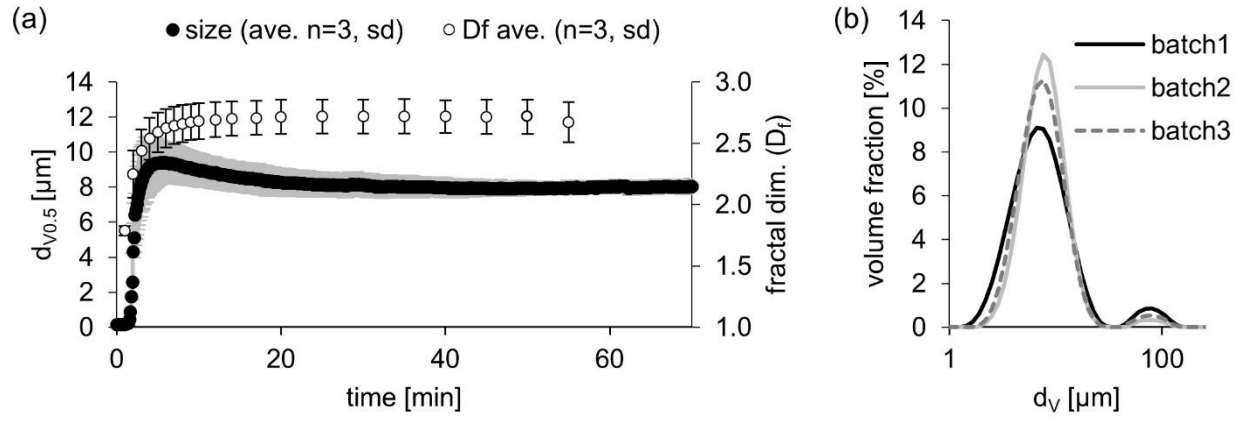

Figure 2. (a) Evolution of volume-based median floc diameters ($d_{V0.5}$) and fractal dimensions (D_f) of three between-batches replicates (ave. ± sd) during floc association (pH 5, 0.1 mM electrolytes); **(b)** respective size distributions at 60 min.

SPM analogue preparation by 24 h *shaker equilibration* was also well reproducible (Figure 3 a), exhibiting within-batch RSDs (n = 4, compared at 60 min) of 11.1 % and 1.4 %, for size (mode d_V = 6.6 µm) and fractal dimension (D_f = 2.65) respectively. Both parameters were similar to freshly associated flocs compared at 60 min (Figure 3 b). For size distributions see Figure S6-2.

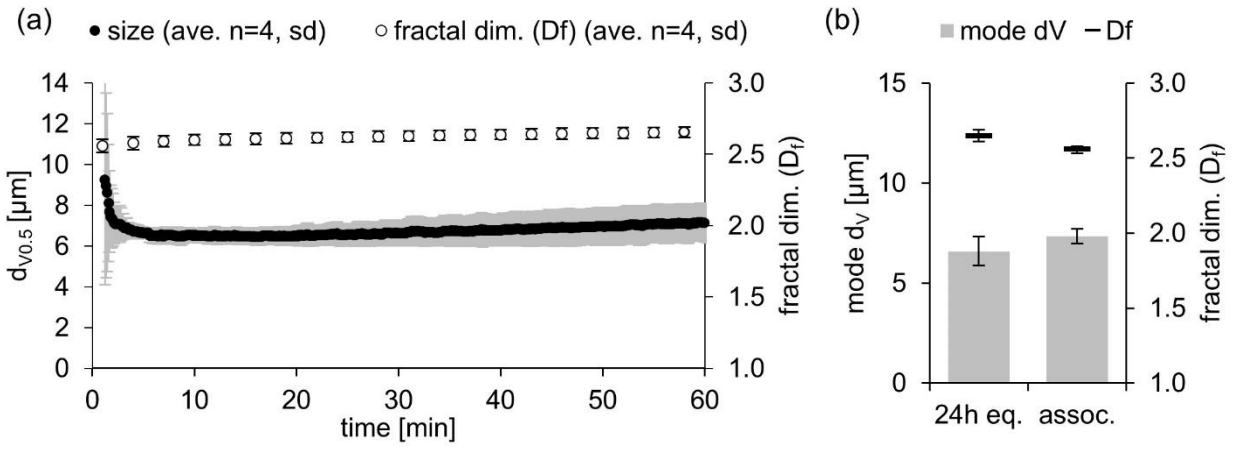

Figure 3. (a) Volume-based median floc diameters ($d_{V0.5}$) and fractal dimensions (D_f) of four within-batch replicates (ave. ± sd) prepared by 24 h *shaker equilibration*; **(b)** Volume-based mode diameters (d_V) and fractal dimensions of four within-batch replicates (ave. ± sd) prepared by *association* and *shaker equilibration* methods (compared at 60 min measurement time).

SEM images (Figure 4 a) show complex SPM analogue floc structures that incorporate all constituents, generating heterogeneous surfaces. Images resemble those of natural SPM (Buffle et al., 1998; Le Meur et al., 2016; Slomberg et al., 2016; Wheatland et al., 2017). With hematite being the smallest and quartz the largest component (Figure 4 b), their relative sizes reflect trends observed for natural SPM, where quartz-shares increase in the larger size fraction and FeOx mainly form nanoparticles or patchy coatings on larger particles (Walch et al., 2022). As expected from

the positive surface charge of hematite (Figure S3-2) in the given hydrochemistry (pH 5, 0.1 mM electrolytes, no SR-NOM), SEM images show hematite to act as bridging-agent between illite and quartz (Figure S6-3). Hematite mainly distributes on the negative edges of illite (Figure S6-4), where it is likely associated with tryptophan, as NOM-FeOx associations seaming clay edges have been previously reported (Poulton and Raiswell, 2005). Quartz mostly distributes on the floc surface, while the core is composed of illite-hematite associations (Figure S6-5). This reflects modelling results (Frungieri et al., 2020) which showed that agglomeration of imbalanced mixtures of positively and negatively charged particles depleted minority particles first, while majority particles cover the agglomerate surface. In our case, positive surface charges (on hematite and illite edges) represent the minority and negative charges (on quartz and illite basal planes) the majority, as confirmed by an overall negative floc zeta potential of -18 ± 1.2 mV.

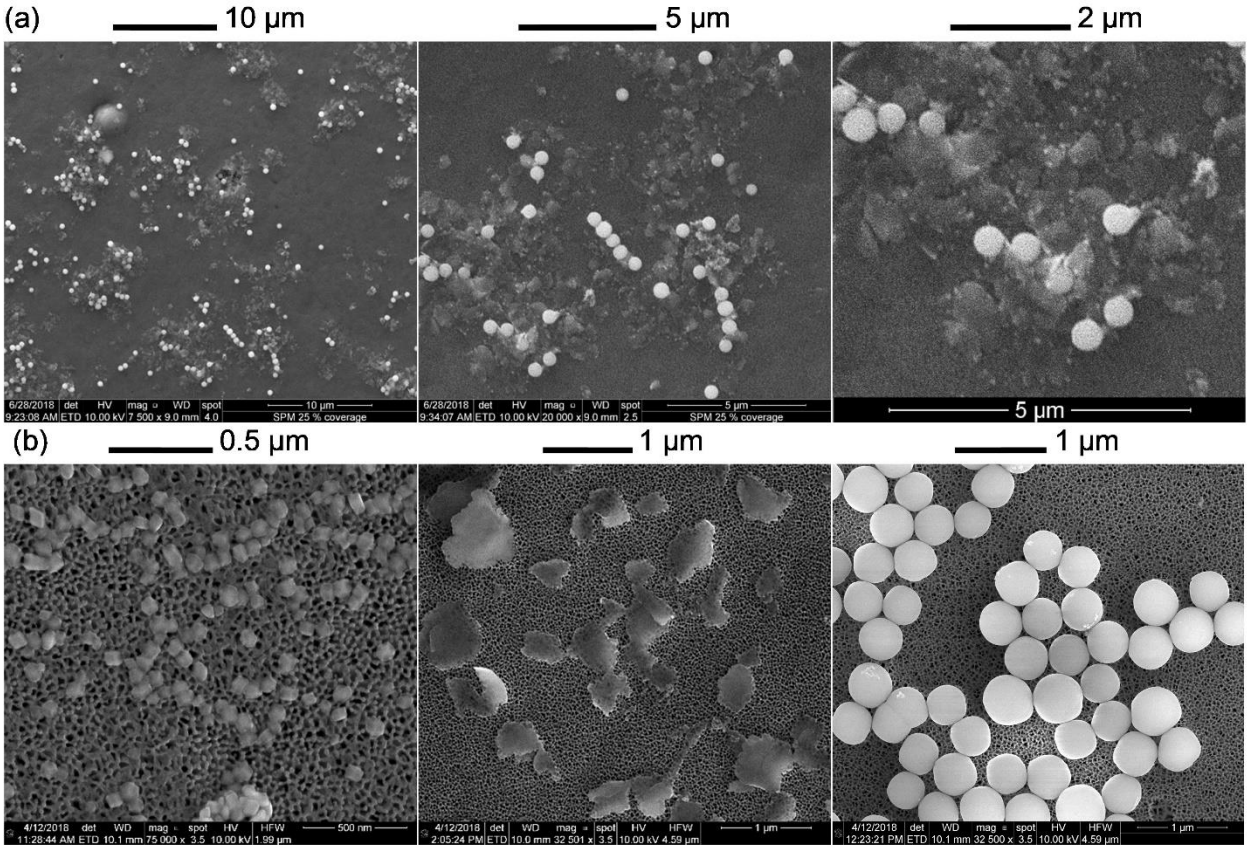

Figure 4. SEM images **(a)** of the SPM analogue flocs at different resolutions and **(b)** of the mineral constituents: hematite, illite and quartz (from left to right).

3.2. Floc Size Evolution is Controlled by Particle Concentration and Stirring Speed.

Floc association and size evolution proceeds in three phases: (1) quick, diffusion-limited association governed by electrostatic forces, (2) a shear and concentration dependent restructuring and compaction phase, (3) further floc growth approaching a flocculation-rupture regime.

Initial association is fueled by a high primary particle number allowing for a high collision frequency. Due to opposite charges of the components (Figure S3-2) in the present hydrochemistry (pH 5, 0.1 mM electrolytes), association is probably diffusion limited (attachment efficiency $\alpha \sim 1$) and attachment governed by electrostatic attractions (neutralization of negative charges on illite

and quartz by addition of positive hematite, Ca^{2+} and Mg^{2+}). Collision-dependance is confirmed by a slower and slightly retarded association at halved concentrations (Figure 5 a). Lower stirring should also reduce collisions but had little impact on the early association phase. This is because the collision rate is proportional to the concentration squared, while proportional to the mean shear rate (Tran et al., 2018). Additionally, all primary particles (quartz, illite, hematite) were nano-sized, and diffusion-driven collisions prevail over orthokinetic (advection-driven) collisions (Figure S7-1 a), resulting in an insignificance of shear (Han and Lawler, 1992; Praetorius et al., 2020).

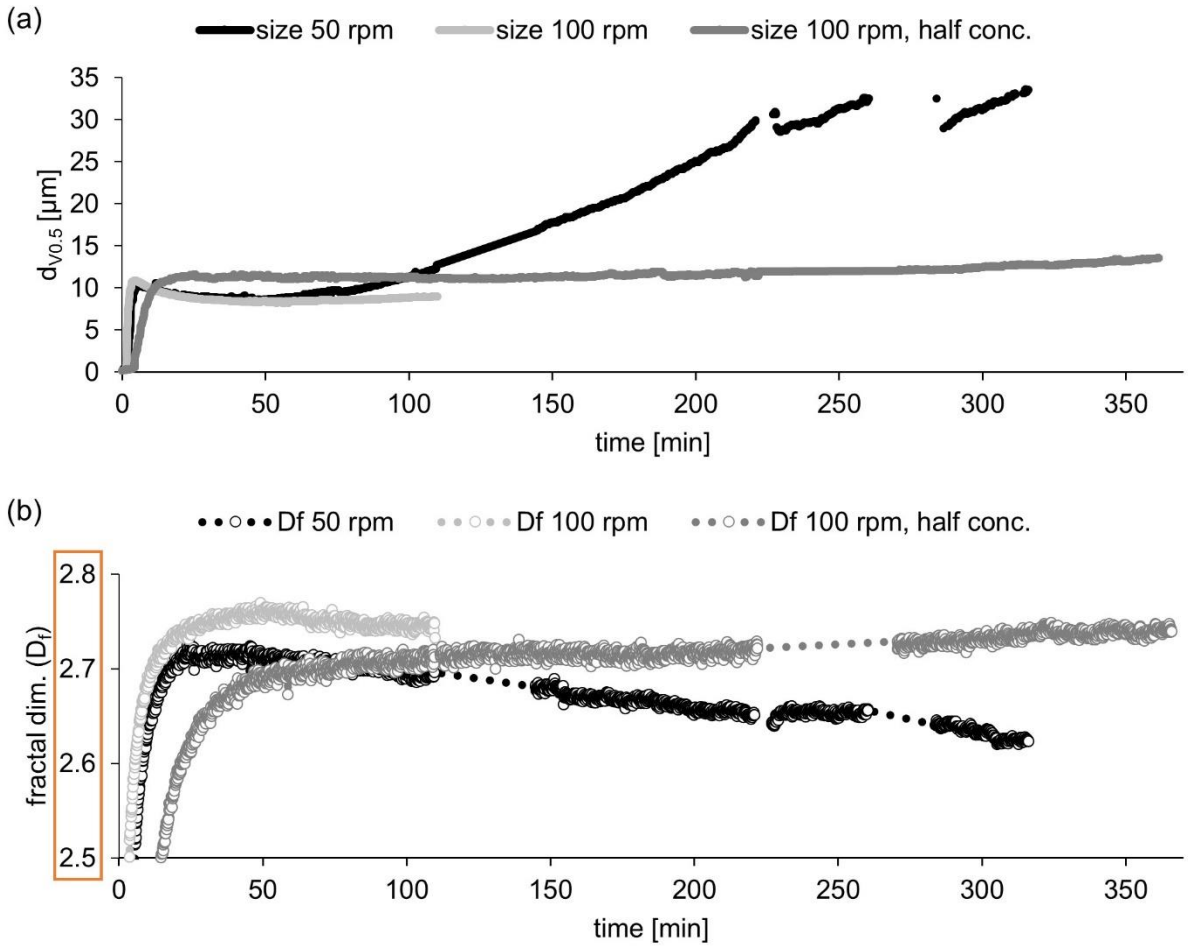

Figure 5. Co-evolution of **(a)** SPM analogue floc size and **(b)** fractal dimension (note the axis zoom), as controlled by stirring speed (shear forces) and SPM concentration.

With a decreasing primary particle number, the collision frequency decreases, while, simultaneously, charge heterogeneities are neutralized, letting floc size plateau. According to the model by Frungieri et al. (2020), size stabilizes when minority particles (in terms of surface charge) are used up and floc surfaces are covered by majority particles, establishing an electrostatic energy barrier. The model showed good stabilization at 85 % majority particles, while growth was self-accelerating at equal shares. A rough calculation of the positive and negative surface areas in the present SPM component mix yields 92.5 % negative and 7.5 % positive surface (Table S7-1).

Since the composition was based on natural SPM composition, future research should address if natural flocs require a certain composition ratio to persist as stable flocs.

At 45 ppm SPM, size peaked and slightly decreased before plateauing (Figure 5 a). Size reduction was suggested to result from floc compaction and restructuring (Selomulya et al., 2003), which is supported by observations of an increase in floc circularity during that phase (Vlieghe et al., 2014). A zoom into the fractal dimension axis (Figure 5 b) reveals that size peaks and dips before D_f reaches its maximum, and D_f continues to slowly increase (indicating compaction) until the floc size plateaus. Restructuring can proceed in two ways: (1) As a consequence of charge neutralization, the attachment efficiency has dropped, and collision energy is dissipated by slowly continued compaction rather than flocculation; (2) Flocs have reached a size-range where shear forces start to act on them and induce restructuring, which was demonstrated by a model by Becker et al. (2009). Since, in the case of halved SPM concentrations, a size peak-dip sequence was not observed, a ballistic effect is more likely than a shear effect.

At some point flocs resume growth (see size at 50 rpm in Figure 5 a) for two possible reasons: (1) floc restructuring reduces the suggested surface enrichment of (negatively charged) majority particles (Frungieri et al., 2020), lowering the electrostatic energy barrier; (2) compaction increases the components' coordination number and floc stability (Conchuir et al., 2014; Selomulya et al., 2003), inhibiting dissipation of collision energy by deformation, and allowing energy barriers to be overcome. When flocculation is resumed, D_f slowly decreases again (see D_f at 50 rpm in Figure 5 b). This coincides with the clear proliferation of a second peak in the size distribution (Figure S7-2), confirming that primary SPM flocs flocculate to larger, again less compact secondary flocs, which finally approach a flocculation-rupture regime (see size at 50 rpm in Figure 5 a) due to shear-induced rupture of loose flocs (Becker et al., 2009).

The extension of the interim size-plateau was clearly shorter at reduced stirring speed (50 instead of 100 rpm) (Figure 5 a). As SPM flocs have reached several µm in size, orthokinetic (advective) collisions dominate (Figure S7-1 b). Lower stirring speed lowers the approach velocity of flocs and thus their mutual repulsion by hydrodynamic effects (Gregory, 2005). As flocs are fractal agglomerates, not solid spheres, a less turbulent flow allows permeation of flocs and induces a transition from curvilinear towards rectilinear floc trajectories, which increases the collision frequency (Bäbler et al., 2006; Han and Lawler, 1992; Li and Logan, 1997; Veerapaneni and Wiesner, 1996). Lower shear stress and lower ballistic stress (Tran et al., 2018) additionally reduce floc rupture and allow for quicker resumption of growth. Halving the concentrations (22.5 instead of 45 ppm SPM) at 100 rpm stirring prolonged the plateauing phase (Figure 5 a), as explained by a reduced collision frequency slowing down compaction and the onset of further floc growth, together with relatively high shear forces sustaining floc rupture and/or hydrodynamic effects – i.e., curvilinearity of collision trajectories.

3.3. SPM Analogues Are Storable, Resilient and Robust upon Resuspension.

Storage and resuspension tests revealed that flocs can be stored for at least 8 d without any significant change in fractal dimension, volume-based diameter (Figure 6), or size distribution (Figure S8-1), no matter if batches were repeatedly resuspended or stored for a certain time without interim resuspension (parallel batches). The different resuspension techniques applied had no impact on floc size after a stabilization time of 60 min (Figure 6 a), while the fractal dimension was generally lower for sonication treatments. The latter reflects observations of partial floc rupture through sonication, and regrowth within the stabilization time. Shaker-resuspended samples, in turn, exhibited breakage of initial larger clusters to original floc size when introduced

into the stirred batch system. Within-treatment RSDs over 8 or 9 storage days ranged from 0.9 % to 1.4 % for D_f and from 4 % (ultrasonic probe) via 5.5 % (shaker) to 13 % (ultrasonic bath) for size ($d_{V0.5}$). At 15 or 20 days of storage, deviations of $d_{V0.5}$ and D_f (Figure 6) as well as size distributions (Figure S8-1) were clearly pronounced for shaker-resuspension. Employing ultrasound, storability may be extended beyond 8 days, close to 20 days.

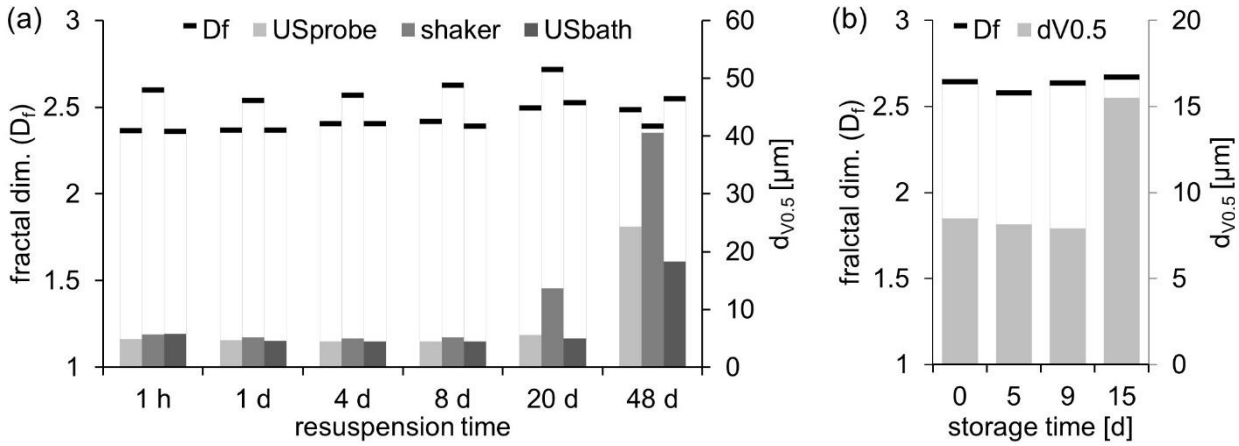

Figure 6. Volume-based median diameter and fractal dimension (D_f) at 60 min measurement time, after resuspension **(a)** of the same three batches at different time intervals by a different treatment each; **(b)** of independent batches resuspended by shaking for 1 h after different storage times each.

Varying stirring speeds (between 50, 100 & 150 rpm) after resuspension (by ultrasonic probe), hardly influenced the volume-based median SPM floc diameter. The RSD of floc size among speeds (compared after 60 min of stirring) was only 7 %, which confirms results of Yu et al. (Yu et al., 2011) showing that, after floc breakage and regrowth, shear conditions had little impact on size. The concentration effect on floc size was also concealed by resuspension. During floc association, halved SPM concentration (22.5 ppm) yielded a higher plateau size (mode

d_V = 11.1 µm) than 45 ppm (mode d_V = 7.3 µm) (Figure S8-2 a). After resuspension, batches prepared at 22.5 and 45 ppm, as well as 45 ppm batches diluted 1:1 (either before, or after 24 h shaking) all approached similar floc sizes when exposed to controlled stirring conditions (100 rpm) in the Mastersizer setup for about 1.5 h (mode d_V = 9.1 - 10.4 µm) (Figure S8-2 b).

3.4. SPM Formation, Size and Fractal Dimension Depend on Hydrochemistry.

When being prepared in the respective target hydrochemistry, not all combinations of electrolyte and SR-NOM concentrations led to floc formation (Figure 7 a). This can be explained by electrostatic stabilization through NOM: SR-NOM is dominated by hydrophobic acids (66-70% of the carbon mass) (Ratpukdi et al., 2009), which are rich in carboxyl groups (IHSS, 2020b; Schumacher et al., 2006). The latter exhibit a low pK_a, making SR-NOM highly negatively charged.

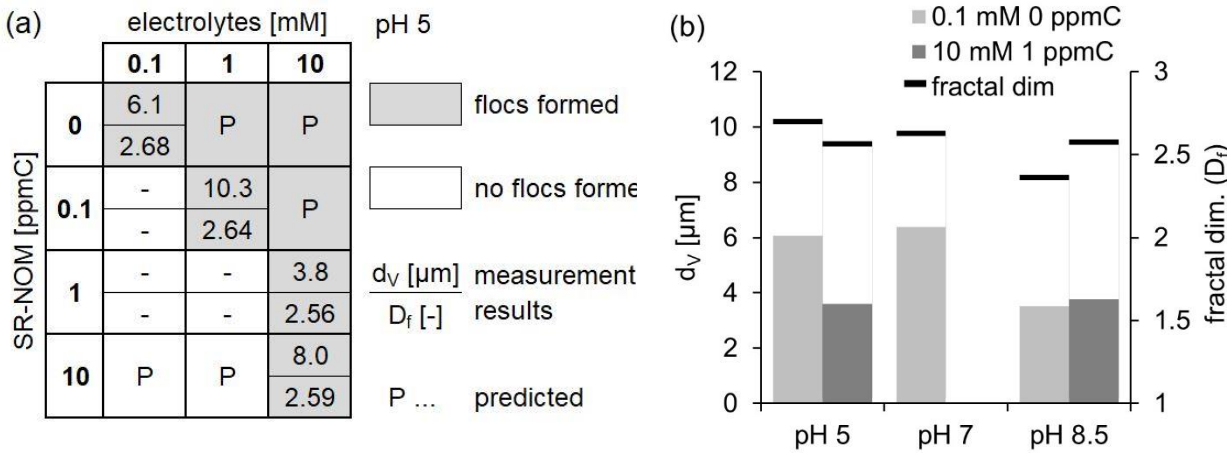

Figure 7. (a) Floc formation by *shaker equilibration* in different hydrochemistries; and **(b)** impact of pH on SPM analogue floc size and fractal dimension.

Electrolytes counteracted NOM-stabilization, and the more SR-NOM was present, the more electrolytes were required to induce flocculation (Figure 7 a). Electrolytes act in several ways: sorption of counterions and strong electrical double layer compression destabilize suspensions (Gregory, 2005), and multivalent ions (especially Ca^{2+}) may induce interparticle bridging (Wang et al., 2017) or bridging flocculation involving NOM (Philippe and Schaumann, 2014) (Figure 1). Combinations of 0.1 mM electrolytes with 0.1 and 1 ppmC SR-NOM, and 1 mM electrolytes with 0.1 ppmC SR-NOM yielded no flocs. This allows to predict that even higher (10 ppmC) SR-NOM concentrations would as well prohibit floc formation at 0.1 mM and 1 mM electrolytes.

Regarding floc size, combined effects of SR-NOM and electrolyte concentrations were not linear. A smaller size of flocs at 10 mM electrolytes with 1 ppmC than with 10 ppmC SR-NOM (Figure 7 a), for example, may either indicate that Ca^{2+}-induced bridging flocculation is limited by SR-NOM concentrations, or that at higher electrolyte concentrations, SO_4^{2-} competes with SR-NOM for sorption sites on hematite (Gu et al., 1995; Tan and Kilduff, 2007). The latter is likely, as both, high electrolytes and SR-NOM strongly reduced or inversed the positive surface charge of hematite (Figure S3-2). An effect of SO_4^{2-} is also supported by a slightly decreasing D_f (from 2.86 down to 2.56) with increasing electrolyte concentrations (Figure 7 a). Of the tested combinations, the largest flocs (at pH 5) resulted at 0.1 ppmC SR-NOM and 1 mM electrolytes (Figure 7 a), concentrations at which hematite was at its isoelectric point (for SR-NOM) or exhibited low positive charge (for electrolytes) (Figure S3-2). Generally, flocculation will be favored by an optimum ratio of SR-NOM, available (favorable) sorption sites, and sorption- or bridging-enhancing electrolyte ions. For mechanistic insights, further research is required.

An impact of pH was observed at low electrolyte concentrations (0.1 mM) and in the absence of SR-NOM (Figure 7 b). Floc compactness (D_f) decreased with increasing pH and finally resulted

in smaller flocs (at pH 8.5), as explained by stronger electrostatic repulsion between SPM components at increasing pH, especially when hematite turns negative at pH 8.5 (Figure S3-2). In presence of 10 mM electrolytes and 1 ppmC SR-NOM, the pH-effect was probably masked by overriding impacts of electrolytes and SR-NOM (Figure 7 b).

3.5. SPM Analogues Remain Stable Upon Transfer into Unfavorable Hydrochemistries

As flocculation was prohibited by some hydrochemical conditions, SPM analogues were generated without any electrolyte or SR-NOM addition (SPMzero) and adjusted to target hydrochemistries unfavorable for flocculation. SPMzero association at pH 5 (positive charge of hematite) yielded a larger plateau floc size at 60 min (mode $d_V = 15.42 \pm 0.96$ µm, within-batch), than flocs associated at 0.1 mM electrolytes (mode $d_V = 7.3 \pm 0.4$ µm), in accordance with hematite being more positively charged in absence of electrolytes (Figure S3-2).

The modification of hydrochemistry to 0.1 mM electrolytes & 1 ppmC SR-NOM in course of a 1:1 dilution of both, freshly associated and overnight shaker-equilibrated SPMzero, did not induce disintegration of flocs (Figures S8-3 and S8-4), even though these hydrochemical conditions prohibited flocculation (Figure 7 a). Agglomeration is frequently reported to not be fully reversible and de-agglomeration by unfavorable hydrochemistry produces fragments rather than single particles (Baalousha, 2009; Loosli et al., 2013; Mohd Omar et al., 2014), as probably mainly weak bonds (secondary minima) are broken (Philippe and Schaumann, 2014; Wang et al., 2016). Still, the extent of de-agglomeration was found to increase with concentration of stabilizing NOM and with reaction time, as molecules slowly migrate into agglomerates (Baalousha et al., 2009; Loosli et al., 2013). However, even after storage for 6 d and resuspension (by shaking over night for >18 h), SPMzero floc integrity was not affected by the modified hydrochemistry and resuspended

flocs approached the sizes of freshly hydrochemistry-adjusted flocs after about 1.5 h in controlled stirring conditions (Figures S8-3 and S8-4). Consequently, after every physical or chemical impact, a conditioning phase in the final experimental stirring conditions should be allowed.

4. Conclusions

In this study we developed SPM analogues which can be used to investigate interactions of SPM with particulate contaminants, such as engineered nanomaterials, nano- and microplastics, soot, or others, at environmentally relevant freshwater conditions. Natural SPM composition is complex and characterized by heterogeneous physicochemical surface properties. Hence, interactions of contaminant particles with SPM will be governed by multiple co-occurring interaction mechanisms, which are even more tortuous considering naturally occurring hydrochemistries. While simple test systems are highly important to gain in-depth mechanistic understanding, complexity cannot be neglected when trying to properly represent natural systems and informed simplifications should guide the development of environmentally relevant and standardizable test systems.

Our SPM analogues were designed to represent those physicochemical surface properties of natural SPM relevant for interactions with particulate contaminants. Selected components not only represent the most abundant components of natural riverine SPM in realistic mass-ratios, but also maximize heterogeneity in physicochemical surface properties, and the resultant SPM analogue flocs reflect the complex composition and structure of natural riverine SPM. These analogues could be reproducibly generated at different agitation conditions (shaking, stirring), as association is controlled by surface chemistry.

The primary role of surface chemistry for flocculation was confirmed by inhibition when component surfaces are repulsive in hydrochemistries unfavorable for floc formation. However, flocs associated under favorable conditions did not disintegrate upon subjection to hydrochemistries suppressing flocculation and SPM analogues can be transferred into unfavorable hydrochemistries for follow-up experiments.

For direct use of freshly associated flocs in experiments, the experiment duration should not exceed the extent of the stable size plateau, which depends on shear forces and SPM concentrations in the system. For flocculation conditions tested here, the plateauing phase lasted for at least 1.5 h. While floc association was somewhat sensitive to varying stirring speeds and SPM concentrations, analogues which had sedimented and rested during storage exhibited extended stability and higher robustness to modified stirring speeds and SPM concentrations upon resuspension.

Physical or chemical impacts, such as changed agitation (stirring or shaking), sedimentation and storage, resuspension (by shaking, ultrasonic bath or probe), dilution, or changed hydrochemistry, induced elastic changes, and the SPM flocs returned to a stable size when exposed to controlled stirring for 1 - 1.5 h. The resilience of SPM analogues to sedimentation and resuspension and the storability for at least 8 days eases handling in the lab and allows for flexibility when planning experiments. The flocs also seem to be quite robust to varying stirring speeds. However, if a different agitation regime is employed, stability of size should be reevaluated and may be tuned via stirring speed and SPM concentration.

The presented SPM analogues constitute the missing link between complex natural systems and simplistic approaches, providing the prerequisite for the development of standardizable and yet environmentally relevant experimental protocols to assess the behavior and fate of particulate contaminants in the presence of SPM. Employing these analogues, fate processes like

heteroagglomeration (OECD, 2020), SPM-assisted transport or sedimentation, bioavailability and uptake in the presence of SPM may be investigated in a comparable manner for various types of particulate contaminants.

Author Contributions

The manuscript was written through contributions of all authors. All authors have given approval to the final version of the manuscript. **Helene Walch**: conceptualization, methodology, validation, formal analysis, investigation, writing – original draft, visualization, project administration. **Frank von der Kammer**: conceptualization, methodology, writing – review & editing, supervision, funding acquisition. **Antonia Praetorius**: conceptualization, methodology, writing – review & editing, supervision. **Thilo Hofmann**: resources, writing – review & editing, supervision.

Funding Sources

This work was supported by EU Horizon 2020 project NanoFASE [grant number 646002].

Notes

The authors declare no competing financial interest.

Acknowledgements

We express sincere thanks to Nathalie Tepe, Vesna Micic Batka and Gerlinde Habler for SEM imaging. Financial support from the EU Horizon 2020 project NanoFASE [grant number 646002] is gratefully acknowledged.

References

Abdolahpur Monikh, F., Praetorius, A., Schmid, A., Kozin, P., Meisterjahn, B., Makarova, E., Hofmann, T., von der Kammer, F., 2018. Scientific rationale for the development of an OECD test guideline on engineered nanomaterial stability. NanoImpact 11, 42–50. doi:10.1016/j.impact.2018.01.003

Adam, V., Loyaux-Lawniczak, S., Labille, J., Galindo, C., del Nero, M., Gangloff, S., Weber, T., Quaranta, G., 2016. Aggregation behaviour of TiO2 nanoparticles in natural river water. J. Nanoparticle Res. 18, 13. doi:10.1007/s11051-015-3319-4

Baalousha, M., 2009. Aggregation and disaggregation of iron oxide nanoparticles: Influence of particle concentration, pH and natural organic matter. Sci. Total Environ. 407, 2093–2101. doi:10.1016/j.scitotenv.2008.11.022

Baalousha, M., Lead, J.R., Von Der Kammer, F., Hofmann, T., 2009. Natural Colloids and Nanoparticles in Aquatic and Terrestrial Environments, in: Environmental and Human Health Impacts of Nanotechnology. pp. 109–161. doi:10.1002/9781444307504.ch4

Bäbler, M.U., Sefcik, J., Morbidelli, M., Bałdyga, J., 2006. Hydrodynamic interactions and orthokinetic collisions of porous aggregates in the Stokes regime. Phys. Fluids 18, 013302. doi:10.1063/1.2166125

Baun, A., Sayre, P., Steinhäuser, K.G., Rose, J., 2017. Regulatory relevant and reliable methods and data for determining the environmental fate of manufactured nanomaterials. NanoImpact 8, 1–10. doi:10.1016/j.impact.2017.06.004

Becker, V., Schlauch, E., Behr, M., Briesen, H., 2009. Restructuring of colloidal aggregates in

shear flows and limitations of the free-draining approximation. J. Colloid Interface Sci. 339, 362–372. doi:10.1016/j.jcis.2009.07.022

Buffle, J., Wilkinson, K.J., Stoll, S., Filella, M., Zhang, J., 1998. A Generalized Description of Aquatic Colloidal Interactions: The Three-colloidal Component Approach. Environ. Sci. Technol. 32, 2887–2899. doi:10.1021/es980217h

Conchuir, B.O., Harshe, Y.M., Lattuada, M., Zaccone, A., 2014. Analytical Model of Fractal Aggregate Stability and Restructuring in Shear Flows. Ind. Eng. Chem. Res. 53, 9109–9119. doi:10.1021/ie4032605

Dale, A.L., Lowry, G. V, Casman, E.A., 2015. Much ado about α: Reframing the debate over appropriate fate descriptors in nanoparticle environmental risk modeling. Environ. Sci. Nano 2, 27–32. doi:10.1039/c4en00170b

Droppo, I.G., 2001. Rethinking what constitutes suspended sediment. Hydrol. Process. 15, 1551–1564. doi:10.1002/hyp.228

Eisma, D., 1993. Suspended Matter in the Aquatic Environment. Springer Berlin Heidelberg, Berlin, Heidelberg. doi:10.1007/978-3-642-77722-6

Elimelech, M., Gregory, J., Jia, X., Williams, R.A., 1995. Modelling of aggregation processes, in: Particle Deposition & Aggregation. Elsevier, Woburn, pp. 157–202. doi:10.1016/B978-075067024-1/50006-6

Frungieri, G., Babler, M.U., Vanni, M., 2020. Shear-Induced Heteroaggregation of Oppositely Charged Colloidal Particles. Langmuir 36, 10739–10749. doi:10.1021/acs.langmuir.0c01536

Gallego-Urrea, J.A., Hammes, J., Cornelis, G., Hassellöv, M., 2016. Coagulation and sedimentation of gold nanoparticles and illite in model natural waters: Influence of initial particle concentration. NanoImpact 3–4, 67–74. doi:10.1016/j.impact.2016.10.004

Geitner, N.K., Marinakos, S.M., Guo, C., O'Brien, N., Wiesner, M.R., 2016. Nanoparticle Surface Affinity as a Predictor of Trophic Transfer. Environ. Sci. Technol. 50, 6663–6669. doi:10.1021/acs.est.6b00056

Gregory, J., 2005. Particles in Water. CRC Press, Boca Raton. doi:10.1201/9780203508459

Gu, B., Schmitt, J., Chen, Z., Liang, L., McCarthy, J.F., 1995. Adsorption and desorption of different organic matter fractions on iron oxide. Geochim. Cosmochim. Acta 59, 219–229. doi:10.1016/0016-7037(94)00282-Q

Guo, L., He, Q., 2011. Freshwater flocculation of suspended sediments in the Yangtze River, China. Ocean Dyn. 61, 371–386. doi:10.1007/s10236-011-0391-x

Han, M., Lawler, D.F., 1992. The (Relative) Insignificance of G in Flocculation. J. Am. Water Works Assoc. 84, 79–91. doi:10.1002/j.1551-8833.1992.tb05869.x

Henning, K.-H., Damke, H., Kasbohm, J., Puff, T., Breitenbach, E., Theel, O., Kießling, A., 2001. Schwebstoffbeschaffenheit im Odersystem. Greifswald.

Hofmann, T., von der Kammer, F., 2009. Estimating the relevance of engineered carbonaceous nanoparticle facilitated transport of hydrophobic organic contaminants in porous media. Environ. Pollut. 157, 1117–1126. doi:10.1016/j.envpol.2008.10.022

IHSS, 2020a. Elemental Compositions and Stable Isotopic Ratios of IHSS Samples [WWW

Document]. URL http://humic-substances.org/elemental-compositions-and-stable-isotopic-ratios-of-ihss-samples/ (accessed 1.22.20).

IHSS, 2020b. Acidic Functional Groups of IHSS Samples [WWW Document]. URL http://humic-substances.org/acidic-functional-groups-of-ihss-samples/ (accessed 2.12.20).

Labille, J., Harns, C., Bottero, J.-Y., Brant, J., 2015. Heteroaggregation of Titanium Dioxide Nanoparticles with Natural Clay Colloids. Environ. Sci. Technol. 49, 6608–6616. doi:10.1021/acs.est.5b00357

Lartiges, B.S., Deneux-Mustin, S., Villemin, G., Mustin, C., Barrès, O., Chamerois, M., Gerard, B., Babut, M., 2001. Composition, structure and size distribution of suspended particulates from the Rhine River. Water Res. 35, 808–816. doi:10.1016/S0043-1354(00)00293-1

Le Meur, M., Montargès-Pelletier, E., Bauer, A., Gley, R., Migot, S., Barres, O., Delus, C., Villiéras, F., 2016. Characterization of suspended particulate matter in the Moselle River (Lorraine, France): evolution along the course of the river and in different hydrologic regimes. J. Soils Sediments 16, 1625–1642. doi:10.1007/s11368-015-1335-8

Li, X., Logan, B.E., 1997. Collision frequencies between fractal aggregates and small particles in a turbulently sheared fluid. Environ. Sci. Technol. 31, 1237–1242. doi:10.1021/es960772o

Li, Y., Wang, X., Fu, W., Xia, X., Liu, C., Min, J., Zhang, W., Crittenden, J.C., 2019. Interactions between nano/micro plastics and suspended sediment in water: Implications on aggregation and settling. Water Res. 161, 486–495. doi:10.1016/j.watres.2019.06.018

Loosli, F., Le Coustumer, P., Stoll, S., 2013. TiO2nanoparticles aggregation and disaggregation in

presence of alginate and Suwannee River humic acids. pH and concentration effects on nanoparticle stability. Water Res. doi:10.1016/j.watres.2013.07.021

Mohd Omar, F., Abdul Aziz, H., Stoll, S., 2014. Aggregation and disaggregation of ZnO nanoparticles: Influence of pH and adsorption of Suwannee River humic acid. Sci. Total Environ. 468–469, 195–201. doi:10.1016/j.scitotenv.2013.08.044

OECD, 2020. GD 318: Guidance Document for the testing of dissolution and dispersion stability of nanomaterials and the use of the data for further environmental testing and assessment strategies. Series on Testing and Assessment No. 318. OECD Guidel. Test. Chem. 1–48.

OECD, 2017. Test No. 318: Dispersion Stability of Nanomaterials in Simulated Environmental Media, OECD Guidelines for the Testing of Chemicals, Section 3. OECD, Paris. doi:10.1787/9789264284142-en

Oriekhova, O., Stoll, S., 2018. Heteroaggregation of nanoplastic particles in the presence of inorganic colloids and natural organic matter. Environ. Sci. Nano 5, 792–799. doi:10.1039/C7EN01119A

Perdue, M., 2012. Replenishment of the Reference Suwannee River Natural Organic Matter (NOM). Muncie.

Philippe, A., Schaumann, G.E., 2014. Interactions of Dissolved Organic Matter with Natural and Engineered Inorganic Colloids: A Review. Environ. Sci. Technol. 48, 8946–8962. doi:10.1021/es502342r

Poulton, S.W., Raiswell, R., 2005. Chemical and physical characteristics of iron oxides in riverine

and glacial meltwater sediments. Chem. Geol. 218, 203–221. doi:10.1016/j.chemgeo.2005.01.007

Praetorius, A., Badetti, E., Brunelli, A., Clavier, A., Gallego-Urrea, J.A., Gondikas, A., Hassellöv, M., Hofmann, T., Mackevica, A., Marcomini, A., Peijnenburg, W., Quik, J.T.K., Seijo, M., Stoll, S., Tepe, N., Walch, H., von der Kammer, F., 2020. Strategies for determining heteroaggregation attachment efficiencies of engineered nanoparticles in aquatic environments. Environ. Sci. Nano 7, 351–367. doi:10.1039/C9EN01016E

Praetorius, A., Labille, J., Scheringer, M., Thill, A., Hungerbühler, K., Bottero, J.-Y., 2014a. Heteroaggregation of Titanium Dioxide Nanoparticles with Model Natural Colloids under Environmentally Relevant Conditions. Environ. Sci. Technol. 48, 10690–10698. doi:10.1021/es501655v

Praetorius, A., Tufenkji, N., Goss, K.-U., Scheringer, M., von der Kammer, F., Elimelech, M., 2014b. The road to nowhere: equilibrium partition coefficients for nanoparticles. Environ. Sci. Nano 1, 317–323. doi:10.1039/C4EN00043A

Quik, J.T.K., Velzeboer, I., Wouterse, M., Koelmans, A.A., van de Meent, D., 2014. Heteroaggregation and sedimentation rates for nanomaterials in natural waters. Water Res. 48, 269–279. doi:10.1016/j.watres.2013.09.036

Ratpukdi, T., Rice, J.A., Chilom, G., Bezbaruah, A., Khan, E., 2009. Rapid Fractionation of Natural Organic Matter in Water Using a Novel Solid-Phase Extraction Technique. Water Environ. Res. 81, 2299–2308. doi:10.2175/106143009X407302

Salminen, R., Batista, M.J., Bidovec, M., Demetriades, A., De Vivo, B., De Vos, W., Duris, M.,

Gilucis, A., Gregorauskiene, V., Halamic, J., Heitzmann, P., Lima, A., Jordan, G., Klaver, G., Klein, P., Lis, J., Locutura, J., Marsina, K., Mazreku, A., O'Connor, P.J., Olsson, S.Å., Ottesen, R.-T., Petersell, V., Plant, J.A., Reeder, S., Salpeteur, I., Sandström, H., Siewers, U., Steenfelt, A., Tarvainen, T., 2005. Geochemical Atlas of Europe. Part 1: Background Information, Methodology and Maps. Geological Survey of Finland, Espoo.

Schulze, T., Ulrich, M., Maier, D., Maier, M., Terytze, K., Braunbeck, T., Hollert, H., 2015. Evaluation of the hazard potentials of river suspended particulate matter and floodplain soils in the Rhine basin using chemical analysis and in vitro bioassays. Environ. Sci. Pollut. Res. 22, 14606–14620. doi:10.1007/s11356-014-3707-9

Schumacher, M., Christl, I., Vogt, R.D., Barmettler, K., Jacobsen, C., Kretzschmar, R., 2006. Chemical composition of aquatic dissolved organic matter in five boreal forest catchments sampled in spring and fall seasons. Biogeochemistry 80, 263–275. doi:10.1007/s10533-006-9022-x

Selomulya, C., Bushell, G., Amal, R., Waite, T.D., 2003. Understanding the role of restructuring in flocculation: The application of a population balance model. Chem. Eng. Sci. 58, 327–338. doi:10.1016/S0009-2509(02)00523-7

Slomberg, D.L., Ollivier, P., Radakovitch, O., Baran, N., Sani-Kast, N., Miche, H., Borschneck, D., Grauby, O., Bruchet, A., Scheringer, M., Labille, J., 2016. Characterisation of suspended particulate matter in the Rhone River: insights into analogue selection. Environ. Chem. 13, 804. doi:10.1071/EN15065

Stone, V., Nowack, B., Baun, A., van den Brink, N., von der Kammer, F., Dusinska, M., Handy,

R., Hankin, S., Hassellöv, M., Joner, E., Fernandes, T.F., 2010. Nanomaterials for environmental studies: Classification, reference material issues, and strategies for physico-chemical characterisation. Sci. Total Environ. 408, 1745–1754. doi:10.1016/j.scitotenv.2009.10.035

Surette, M.C., Nason, J.A., 2019. Nanoparticle aggregation in a freshwater river: the role of engineered surface coatings. Environ. Sci. Nano 6, 540–553. doi:10.1039/C8EN01021H

Svendsen, C., Walker, L.A., Matzke, M., Lahive, E., Harrison, S., Crossley, A., Park, B., Lofts, S., Lynch, I., Vázquez-Campos, S., Kaegi, R., Gogos, A., Asbach, C., Cornelis, G., von der Kammer, F., van den Brink, N.W., Mays, C., Spurgeon, D.J., 2020. Key principles and operational practices for improved nanotechnology environmental exposure assessment. Nat. Nanotechnol. 15, 731–742. doi:10.1038/s41565-020-0742-1

Tan, Y., Kilduff, J.E., 2007. Factors affecting selectivity during dissolved organic matter removal by anion-exchange resins. Water Res. 41, 4211–4221. doi:10.1016/j.watres.2007.05.050

Tran, D., Kuprenas, R., Strom, K., 2018. How do changes in suspended sediment concentration alone influence the size of mud flocs under steady turbulent shearing? Cont. Shelf Res. 158, 1–14. doi:10.1016/j.csr.2018.02.008

Veerapaneni, S., Wiesner, M.R., 1996. Hydrodynamics of Fractal Aggregates with Radially Varying Permeability. J. Colloid Interface Sci. 177, 45–57. doi:10.1006/jcis.1996.0005

Velzeboer, I., Quik, J.T.K., van de Meent, D., Koelmans, A.A., 2014. Rapid settling of nanoparticles due to heteroaggregation with suspended sediment. Environ. Toxicol. Chem. 33, 1766–1773. doi:10.1002/etc.2611

Vlieghe, M., Coufort-Saudejaud, C., Frances, C., Liné, A., 2014. In situ characterization of floc morphology by image analysis in a turbulent Taylor-Couette reactor. AIChE J. 60, 2389–2403. doi:10.1002/aic.14431

Walch, H., von der Kammer, F., Hofmann, T., 2022. Freshwater suspended particulate matter—Key components and processes in floc formation and dynamics. Water Res. 220, 118655. doi:10.1016/j.watres.2022.118655

Wang, Hao, Zhao, X., Han, X., Tang, Z., Liu, S., Guo, W., Deng, C., Guo, Q., Wang, Huanhua, Wu, F., Meng, X., Giesy, J.P., 2017. Effects of monovalent and divalent metal cations on the aggregation and suspension of Fe3O4 magnetic nanoparticles in aqueous solution. Sci. Total Environ. 586, 817–826. doi:10.1016/j.scitotenv.2017.02.060

Wang, W., Howe, J.Y., Gu, B., 2008. Structure and Morphology Evolution of Hematite (α-Fe 2 O 3) Nanoparticles in Forced Hydrolysis of Ferric Chloride. J. Phys. Chem. C 112, 9203–9208. doi:10.1021/jp800683j

Wang, Z., Jin, Y., Shen, C., Li, T., Huang, Y., Li, B., 2016. Spontaneous Detachment of Colloids from Primary Energy Minima by Brownian Diffusion. PLoS One 11, e0147368. doi:10.1371/journal.pone.0147368

Westerhoff, P., Nowack, B., 2013. Searching for Global Descriptors of Engineered Nanomaterial Fate and Transport in the Environment. Acc. Chem. Res. 46, 844–853. doi:10.1021/ar300030n

Wheatland, J.A.T., Bushby, A.J., Spencer, K.L., 2017. Quantifying the Structure and Composition of Flocculated Suspended Particulate Matter Using Focused Ion Beam Nanotomography.

Environ. Sci. Technol. 51, 8917–8925. doi:10.1021/acs.est.7b00770

Woodward, J.C., Walling, D.E., 2007. Composite suspended sediment particles in river systems: their incidence, dynamics and physical characteristics. Hydrol. Process. 21, 3601–3614. doi:10.1002/hyp.6586

Yu, S., Li, Q., Shan, W., Hao, Z., Li, P., Liu, J., 2021. Heteroaggregation of different surface-modified polystyrene nanoparticles with model natural colloids. Sci. Total Environ. 784, 147190. doi:10.1016/j.scitotenv.2021.147190

Yu, W., Gregory, J., Campos, L., Li, G., 2011. The role of mixing conditions on floc growth, breakage and re-growth. Chem. Eng. J. 171, 425–430. doi:10.1016/j.cej.2011.03.098

Zhou, D., Abdel-Fattah, A.I., Keller, A. a, 2012. Clay Particles Destabilize Engineered Nanoparticles in Aqueous Environments. Environ. Sci. Technol. 46, 7520–7526. doi:10.1021/es3004427

Zimmermann-Timm, H., 2002. Characteristics, Dynamics and Importance of Aggregates in Rivers - An Invited Review. Int. Rev. Hydrobiol. 87, 197–240. doi:10.1002/1522-2632(200205)87:2/3<197::AID-IROH197>3.0.CO;2-7

SUPPORTING INFORMATION

Generation of Reproducible Model Freshwater Particulate Matter Analogues to Study the Interaction with Particulate Contaminants.

Helene Walch [a, 1], *Antonia Praetorius* [a, b], *Frank von der Kammer* [a, *], *Thilo Hofmann* [a, *]

[a] Department of Environmental Geosciences, Centre for Microbiology and Environmental Systems Science, University of Vienna, Althanstraße 14, UZA II, 1090 Vienna, Austria

[b]Department of Ecosystem & Landscape Dynamics, Institute for Biodiversity and Ecosystem Dynamics, University of Amsterdam, Science Park 904, 1098 XH Amsterdam, The Netherlands

h.walch@gmx.at, a.praetorius@uva.nl, frank.kammer@univie.ac.at, thilo.hofmann@univie.ac.at

[*] Corresponding authors: Thilo Hofmann and Frank von der Kammer

---

[1] Present Address: Studies & Consulting, Laboratories, Environment Agency Austria, Spittelauer Lände 5, 1090 Vienna, Austria, helene.walch@umweltbundesamt.at

S1 – Conceptual Framework for SPM Analogue Component Selection

The present conceptual considerations constitute the framework for tailoring suspended particulate matter (SPM) analogues that represent those characteristics of natural riverine SPM which are relevant for interactions with particulate contaminants. Pinpointing these process-relevant characteristics requires informed simplifications (Praetorius et al., 2013) based on a thorough scientific understanding of both the mechanisms governing the affinity of particulate contaminants for SPM, and the intrinsic complexity of SPM. Considering the diversity of possible interaction mechanisms and drivers involved (see main text Figure 1), a realistic test-system for heteroagglomeration needs to account for relevant hydrochemical parameters and SPM physicochemical (surface) characteristics. This requires covering different minerals, that increase surface charge heterogeneities and induce various van der Waals and hydrophobic attractions, as well as the inclusion of relevant (multivalent) electrolyte ions, different types of NOM, and adjustment of pH to enable realistic hydrochemical modulation of particulate contaminant and SPM surface chemistry.

To select the most suitable constituents for SPM analogue generation, we accounted for: (1) factors controlling interactions between particulate contaminants and SPM, (2) typical components and composition-ratios of natural SPM, and (3) components contributing characteristics relevant for interaction mechanisms.

Material Properties and Hydrochemistry Control Particulate Contaminant Attachment to SPM. As summarized by Praetorius et al. (2020) based on particle agglomeration theory (Elimelech et al., 1995; Gregory, 2005), interactions between particulate contaminants and SPM can be

considered a two-step process: a collision step, followed by an attachment step. After collision – by diffusion, differential settling, or advective transport – attachment depends on short-range physicochemical attractive and repulsive forces. Their net effect yields the probability of attachment, referred to as attachment efficiency (α). The attachment efficiency constitutes a direct measure of the physicochemical affinity between contaminant particle and SPM under given conditions and is considered a suitable fate descriptor for particulate contaminants. Since particle interaction forces arise from the interplay of intrinsic material properties and the surrounding hydrochemistry (see main text Figure 1), both need to be well represented in relevant aspects.

Factors influencing attachment have been thoroughly studied, reviewed, and partly incorporated into agglomeration theory (e.g. DLVO) (Baalousha, 2016; Elimelech et al., 1995; Grasso et al., 2002; Gregory, 2005; Hotze et al., 2010; Peijnenburg et al., 2015; Petosa et al., 2010; Sharma et al., 2021; Wang et al., 2015; X. Wang et al., 2021). The major forces involved (see main text Figure 1) are electrostatic, van der Waals and hydrophobic forces, which are material-dependent and modulated by the surrounding hydrochemistry through surface interactions with electrolyte ions, protons or natural organic matter (NOM). The latter is also involved in bridging and steric effects.

Electrostatic forces induce potential long-range particle interactions. They arise from the particle surface charge, resulting from the dissolution of surface constituent ions, ionizable surface functional groups (pH-dependent, variable charge), or isomorphic substitutions in the crystal lattice (permanent charge). Opposite charges induce attraction and same charges repulsion. In the latter case short-range forces, mainly van der Waals and hydrophobic attractions, may outcompete electrostatic repulsion, once particles get close enough due to kinetic forces, or when particle surface charge gets compensated. (Gregory, 2005; Hotze et al., 2010; Petosa et al., 2010)

In aqueous systems surface charge is compensated by counterions, forming an electrical double layer (EDL). Non-specifically interacting ions shield particle surface charge with an efficiency related to ion-valency (Schulze-Hady rule), inducing a compression of the EDL (reduction of Debye length). Specific adsorption of ions and pH-dependent protonation/deprotonation of surface functional groups directly modify the surface charge, yielding a charge increase/reduction, neutralization, or reversal. Reduction/neutralization of surface charge, compression of the EDL, as well as bridging favor interactions with otherwise electrostatically repelled particles or NOM. (Baalousha, 2016; Elimelech et al., 1995; Gregory, 2005; Philippe and Schaumann, 2014)

Multivalent cations (mainly Ca^{2+}) can serve as bridges between particles (Wang et al., 2017) or between particles and (mostly carboxyl-rich) NOM, enhancing bridging-flocculation, while multivalent anions (e.g., SiO_4^{4-}, PO_4^{3-}, SO_4^{2-}, CO_3^{2-}) may compete with NOM for sorption sites (Philippe and Schaumann, 2014), hindering NOM-bridging. (Multivalent anions, however, strongly favor agglomeration of positively charged particles (Walsch and Dultz, 2010; J. Wang et al., 2021)). A low pH as well favors (bridging-)interactions with NOM, by enhancing hydrophobic forces, H-bonding, and ligand-exchange between NOM carboxyl-groups and mineral hydroxyl-groups. However, H^+ competition with Ca^{2+} for complexation sites may counteract cation bridging. (Grasso et al., 2002; Philippe and Schaumann, 2014; Yu et al., 2018).

The role of NOM in particle interactions (see main text Figure 1) depends on properties of the NOM, such as molecular weight (MW), rigidity, conformation, charge density, and hydrophobicity, which are in turn impacted by hydrochemistry (e.g., pH, electrolytes) (Baalousha, 2016; Buffle et al., 1998; Carnal et al., 2015; Grillo et al., 2015; Kunhi Mouvenchery et al., 2012; Petosa et al., 2010; Philippe and Schaumann, 2014; Wang et al., 2015). Adsorbed high-MW NOM molecules, if rigid, can extend beyond particle's repulsive EDL-forces and induce bridging-

flocculation. In case of full particle surface coverage, however, they may induce steric hindrance towards agglomeration. Flexible high-MW molecules flatly sorb to the surface, as they change conformation upon sorption, and, just like low-MW molecules, do not extend beyond the EDL, which excludes bridging. As they can still modify the particle's surface charge, their agglomeration behavior depends on their molecular charge densities and the degree of particle surface coverage: charge heterogeneities through patchy surface coverage (electrostatic patches), and surface charge neutralization through full coverage with molecules of moderate charge densities favor agglomeration, while full coverage with highly charged NOM favors stabilization. (Baalousha, 2016; Buffle et al., 1998; Gregory, 2005; Philippe and Schaumann, 2014)

Relevant Hydrochemical Parameters Can Be Adopted from OECD TG 318.

The representation of hydrochemical river water parameters relevant for particle interactions has been recently operationalized within the OECD test guideline No. 318 *Dispersion stability of nanomaterials in simulated environmental media* (OECD, 2017). The parameters selected – electrolyte composition, dissolved NOM and pH – cover those most strongly affecting the stability of nanomaterials. Since hydrochemical effects on the attachment of contaminant-particles to SPM are governed by the same principles, the rationale beyond the OECD *alternative test medium* composition (Abdolahpur Monikh et al., 2018) is directly applicable to a test system for heteroagglomeration. Electrolyte composition is represented by $Ca(NO_3)^2$ and $MgSO_4$ at a molar ratio of 4:1, which reflects the median composition of 808 European stream waters covered in the FOREGS Geochemical Atlas of Europe (Salminen et al., 2005) regarding Ca^{2+}, Mg^{2+} and SO_4^{2-} concentrations (Abdolahpur Monikh et al., 2018). To account for dissolved NOM, Suwannee River NOM (SR-NOM) standard material is employed. This complements the test system with a rather

refractory humic substances (HS) rich type NOM, rich in carboxylic acids (IHSS, 2020; Ratpukdi et al., 2009; Schumacher et al., 2006).

Component Selection Reflects Process-Relevant Characteristics of Natural Riverine SPM. Riverine SPM can be described as complex and heterogeneous. Complex regarding the assemblage of various organic and inorganic constituents in dynamic floc or agglomerate structures, and heterogeneous regarding the physicochemical surface properties of these constituents and their assembly within the floc. Moreover, spatial and temporal variabilities in SPM concentration, composition, structure, and size intricate the system (Walch et al., 2022), making it impossible to find analogues that represent SPM in all its facets (Praetorius et al., 2020). The heterogeneity in physicochemical surface properties of natural riverine SPM appears to be the most relevant characteristic to be represented by analogues. Each SPM constituent contributes specific physicochemical surface properties to an SPM floc, resulting in an overall heterogeneity, which allows for various interaction mechanisms (see main text Figure 1). Theoretically, each interaction site comes with a distinct probability of attachment, i.e. a different attachment efficiency (α) (Praetorius et al., 2020). As different pathways occur simultaneously, the fate of particulate contaminants will be governed by the dominant interactions. Hence, the component selection was targeted to not only cover the most abundant constituents of natural SPM but also increase the heterogeneity in physicochemical surface properties.

Phyllosilicates and quartz are omnipresent in natural riverine SPM and were selected to account for the most abundant minerals. Together they represent about one third up to more than 90 % of the mineral SPM fraction, with their relative shares ranging from 88:12-45:55. Constituting about 50% of the phyllosilicate mass and a quarter of the total mineral mass in SPM, illite qualified for

representation of the phyllosilicate fraction. Another mineral class we found essential including are iron oxides and (oxy)hydroxides (FeOx). Despite being less abundant in mass, they are quasi omnipresent as nano-sized particles or patchy precipitates on other mineral surfaces (mainly aluminosilicates) and were concluded to play a crucial structural-functional role acting as a cement in SPM flocs. Among the most frequently reported FeOx are amorphous Fe-oxyhydroxides, ferrihydrite, goethite and hematite. (Walch et al., 2022). We selected hematite to represent FeOx, as it can be easily synthesized yielding a well-defined shape and size.

Besides reflecting the typical composition of riverine SPM, illite, quartz and hematite cover a variety of physicochemical surface properties relevant for interactions with contaminant particles. At typical freshwater pH ranges, quartz is highly negatively charged, with points of zero charge mostly at pH < 4, while hematite contributes positive surface charge, with points of zero charge typically at pH > 7 (Kosmulski, 2014, 2001). Illite features intrinsic surface charge heterogeneity: its basal planes are permanently negatively charged due to isomorphic substitutions in the crystal lattice (Si^{4+} in tetrahedral and Al^{3+} in octahedral layers, are substituted by Al^{3+} and Mg^{2+} or Fe^{2+}, respectively), and hydroxyl-groups on broken edges exhibit pH-dependent variable charge (Preocanin et al., 2016). The three materials come with different Hamaker constants (A_{11} in water: 0.8-1.2 × 10^{-20} J for quartz; 3.3-3.9 × 10^{-20} J for FeOx (Baalousha, 2016); 2.5-3.3 × 10^{-20} for illite (Novich and Ring, 1985; Séquaris, 2010; Shao et al., 2020)), and different hydrophobicity, with quartz being hydrophilic and hematite slightly hydrophobic up to neutral pH, at alkaline pH hydroxylation renders it hydrophilic (Shrimali et al., 2016; Tarasevich et al., 2002). Phyllosilicates exhibit hydrophilic and hydrophobic properties (Bantignies et al., 1997; Cuadros, 2017): with a decreasing degree of isomorphic substitution (which is intermediate for illite: talc < kaolinite <

illite < muscovite < montmorillonite) basal planes increase their hydrophobicity, while edge hydroxyl-groups are typically hydrophilic (Yin, 2012).

A considerable mass fraction of natural SPM is organic matter, comprising aquagenic and pedogenic materials ranging from the molecular level, via detrital fragments up to living microorganisms. Particulate organic carbon (POC) contents in SPM typically range between 0.7-16 $\%_{wt}$ with a median of ~4 $\%_{wt}$. Two functional types of NOM are distinguished: extracellular polymeric substances (EPS), and pedogenic humic substances (HS). Although refractory HS mostly dominate the POC fraction, EPS are considered more relevant for SPM floc formation (Walch et al., 2022). This is because EPS include a range of molecular weights, various degrees of charge, hydrophobicity and rigidity (Flemming and Wingender, 2010). Their heterogenous properties render EPS overall more *sticky* than HS, which becomes apparent as strong flocculation coincides with high microbial production and SPM is enriched in labile EPS (Walch et al., 2022).

Labile EPS-type POC is dominated by protein-like substances and carbohydrates with quasi equal shares. Several substances of these two classes were tested (supporting information S2) and the amino acid tryptophan was chosen. Tryptophan (Figure S2 - 1) is a small molecule with a MW of 204.2 g mol^{-1}, which excludes bridging flocculation, but introduces molecular-level charge heterogeneity. Its amino (pKa ~10) and carboxyl group (pKa ~3) make it a zwitterion at environmentally relevant pH. Furthermore, the aromatic side chain is considered non-polar and hydrophobic, while the aliphatic part is hydrophilic, resulting in an amphiphilic character. Tryptophan, thus, seems to well reflect the heterogeneous physicochemical properties of natural EPS, albeit not covering the bridging function of high-MW molecules.

S2 – Screening for EPS Proxy and SPM Analogue Composition Ratios

EPS is mainly composed of polysaccharidic and protein-like molecules (Flemming and Wingender, 2010; Ittekkot and Laane, 1991; Mannino and Harvey, 2000). Since EPS cannot easily be isolated from natural samples, studies frequently employ model polysaccharides extracted from microbial cultures (Filella, 2007). These are typically substances of commercial interest, such as alginate, xanthan, pullulan, dextran, polygalacturonic acid, succinoglycan, schizophyllan, xylinan, gellan, curdlan, scleroglucan, or cyanobacterial polysaccharides (Ates, 2015; Filella, 2007; Morris and Harding, 2009). Moreover, molecular-level identification of NOM/EPS within natural waters is scarce. Regarding proteins, Lee et al. identified tryptophan-like and tyrosine-like compounds in riverine DOM (Lee et al., 2017, 2019) and amino acid analysis of NOM revealed the dominance of neutral amino acids (mainly glycine & alanine), followed by hydroxyl-carrying (serine & threonine) and acidic amino acids (aspartic & glutamic acid) (Artemyev, 1996; Mannino and Harvey, 2000). To choose a suitable EPS proxy for SPM analogue generation, screening tests involved substances selected based on availability and structural considerations, aiming at inclusion of molecules of different MW, charge, and flexibility. Na-alginate (Alg) and xanthan gum (Xan) from Sigma-Aldrich and pullulan (Pull) from Alfa Aesar served as carbohydrate-type proxies. Sigma-Aldrich L-tryptophan (Tryp) and L-glutathione (Glu, a tripeptide composed of glutamic acid, glycine and cysteine) served as protein-like proxies. Additionally, exudates extracted from a Chlamydomonas green algae culture (Chla), provided by Jeffrey A. Nason (Oregon State University, USA), were tested. The structures of the commercial molecules are shown in Figure S2 - 1.

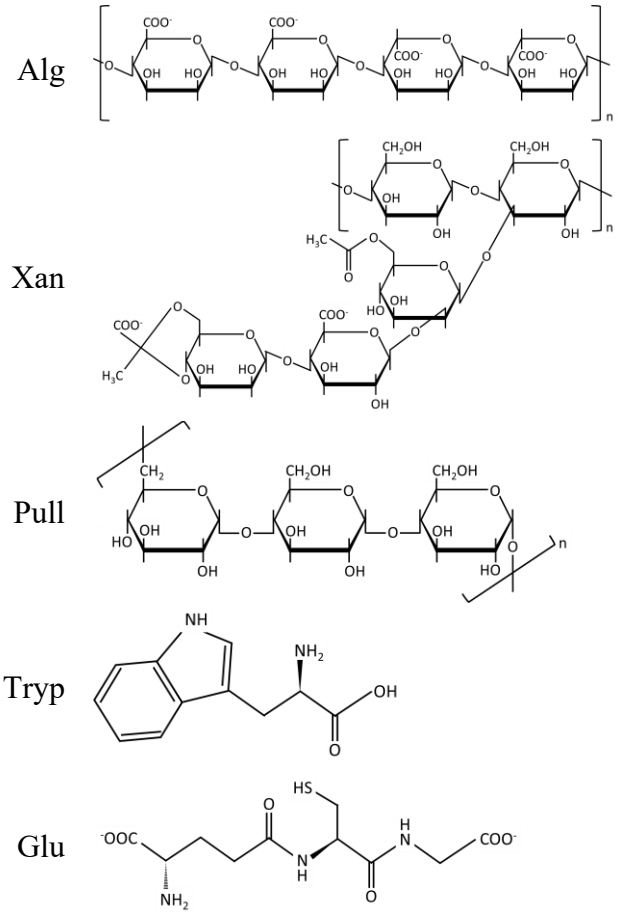

Figure S2 - 1. Molecular structures of EPS proxy molecules

Screening tests involved SPM analogue generation in 100 mL beakers on a 15 places magnetic stirrer operating at 400 rpm. Quartz (Qua), illite (Ill), and hematite (Hem) suspensions, and solutions of the respective EPS proxy and/or 0.1 mM electrolytes ($CaCl_2$ and $MgSO_4$ in a 4:1 molar ratio) were spiked into ultrapure water in different sequences (seq. 1: EPS-Qua-Ill-Hem-electrolytes; seq. 2: Qua-Ill-Hem-electrolytes-EPS; seq. 3: electrolytes-EPS-Qua-Ill-Hem). To select a suitable SPM analogue composition, component ratios were varied within the ranges typical of natural SPM, which revealed phyllosilicate:quartz ratios of 55:45 - 88:12, an FeOx content up to 8 $\%_{wt}$ and POC contents of 0.7 - 16 $\%_{wt}$ (with about 4 - 71 % being labile EPS-like)

(Walch et al., 2022). The Ill:Qua mass-ratio was varied between 55:45, 80:20, and 100:0, and hematite accounted for 0, 0.3, 3.5, 7 or 15 $\%_{wt}$ of the total mineral mass, which was kept constant at 65 ppm. EPS proxy additions, based on the organic carbon contents, varied between 0.8, 4.5 or 9 $\%_{wt}$ of the total mineral mass. After stirring overnight, aliquots of 1 mL were transferred into cuvettes (DTS0012, Malvern) for size measurement on the Malvern Zetasizer Nano ZS. The pH value was not adjusted and naturally varied between 5.3 and 6.3. At that pH range, quartz and illite are overall negatively charged, whereas hematite is positively charged (see Figure S3 - 2).

The plain mineral mix showed an increasing destabilization and agglomerate size with increasing Hem addition (at 15 $\%_{wt}$ Hem, sedimentation during the measurement occurred) (Figure S2 - 2 a). The mechanism appears to be a combination of charge reduction, as a decreasing negativity of zeta potential (ZP) with increasing Hem shows, and bridging of the negatively charged illite/quartz by positively charged Hem particles, as the onset of agglomeration despite still highly negative ZP values in the absence of electrolytes suggests (Figure S2 - 2 b). The addition of 0.1 mM electrolytes enhanced charge compensation and further increased size (Figure S2 - 2 a & b). The effect on size is not visible at 15 % Hem, as sedimentation occurred during the measurement.

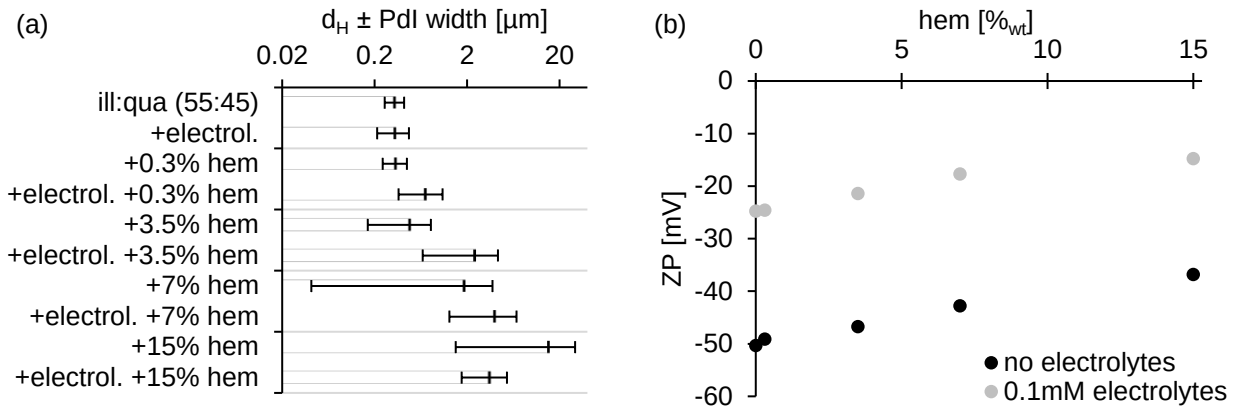

Figure S2 - 2. Size (a) and ZP (b) of SPM prepared at Ill:Qua 55:45 with and without 0.1 mM electrolytes and varying Hem additions (seq.2: Qua-Ill-Hem-electrolytes)

The addition of EPS decreased the floc size of the plain mineral mix (Ill:Qua 55:45, Hem 7 $\%_{wt}$ at 0.1 mM electrolytes) to an extent that depended more the EPS type than on concentration (Figure S2 - 3 a). Alg and Xan inhibited agglomeration by Hem, even at the lowest concentration. Pull, Tryp and Glu compromised the floc size to a lesser extent and narrowed the polydispersity index (PdI) as compared to the pure mineral mix. While Pull exhibited higher variability, Tryp and Glu yielded uniform narrow size distributions, irrespective of concentration.

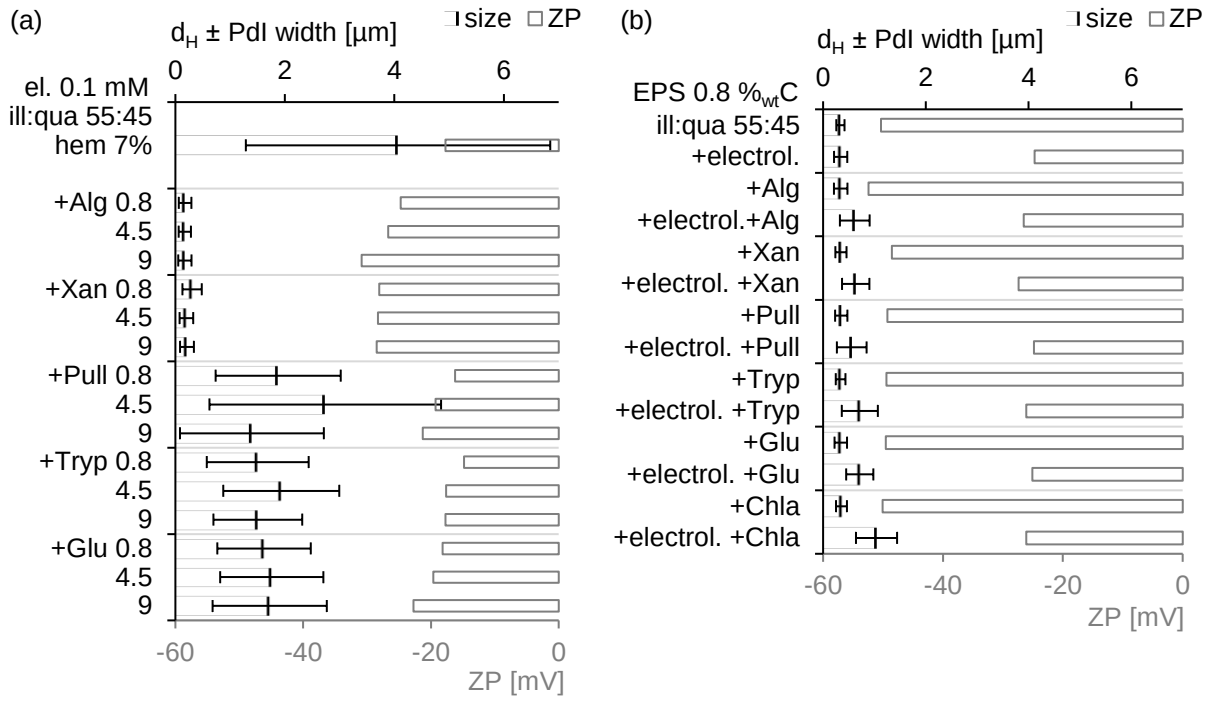

Figure S2 - 3. SPM floc size and ZP at Ill:Qua 55:45 **(a)** with different EPS concentrations at 7 $\%_{wt}$ Hem and 0.1 mM el. (seq. 1: EPS-Qua-Ill-Hem-electrolytes), **(b)** with and without 0.1 mM electrolytes and/or 0.8 $\%_{wt}$C of different EPS (sequence of addition: Qua-Ill-EPS-electrolytes)

Differences among EPS can be related to their molecular characteristics: Alg and Xan carry a high density of negatively charged ($pK_a < 5$) carboxyl-groups (Table S2 - 1, Figure S2 - 1). Hence, their sorption lowered the ZP, inducing stabilization of the SPM components (Figure S2 - 3 a). Since Alg has a low MW and is semi-flexible (Tombs and Harding, 1997), while Xan exhibits a much higher MW and rigid rod-like helical structure (Camesano and Wilkinson, 2001; Tombs and Harding, 1997), steric effects may have co-occurred in the case of Xan especially at higher concentrations (potentially full surface coating). Tryp and Glu are low-MW molecules and carry both, negatively charged carboxyl as well as positively charged amino groups (Table S2 - 1), while Pull is a quasi-neutral (OH-groups with $pK_a > 9$) and flexible molecule (Tombs and Harding,

1997), which are prone to flat adsorption (Buffle et al., 1998). These molecules will neither induce bridging, as they will not extend beyond the electrical double layer, nor electrostatic stabilization, as reflected by the ZPs being hardly modified (Figure S2 - 2 b). Consequently, they decrease the charge effect of Hem, most probably due to preferential adsorption to Hem (Walch et al., 2022), and narrow down SPM floc size without stabilizing single components.

Table S2 - 1. Molecular weights and functional groups (per carbon atom) of EPS proxy substances.

		pK_a	<5	>9	>10
	MW [g/mol]		**COOH/C**	**OH/C**	**NH_2/C**
Alg	214.1		0.17	0.33	
Xan	933.7		0.09	0.31	
Pull	574.6		0.00	0.78	
Tryp	204.2		0.09		0.09
Glu	307.3		0.20		0.10

Without hematite (i.e. the preferential sorbent) present, a combined low addition of EPS (0.8 $\%_{wt}$) and electrolytes (0.1 mM) initiated some agglomeration of illite and quartz (55:45) irrespective of EPS type (Figure S2 - 3 b). Mere electrolyte or EPS effects can be excluded, as neither the addition of electrolytes nor EPS alone triggered agglomeration. Moreover, the ZP change by electrolyte addition was the same (from -50 ± 1 to -26 ± 1 mV), irrespective of EPS presence or type. Agglomeration is, thus, ascribed to specific interactions of EPS with multivalent electrolyte ions (especially Ca^{2+}). The latter can (1) mediate sorption of organic molecules to (negatively charged) mineral surfaces and induce EPS-ion-bridging (Philippe and Schaumann, 2014) or charge heterogeneities (in the case of amino-group carrying Tryp or Glu); (2) favor the formation of supramolecular structures via intermolecular cross-linking (Kunhi Mouvenchery et

al., 2012); and (3) induce structural stabilization of EPS molecules increasing their rigidity (Buffle et al., 1998). All these processes support flocculation.

For Alg and Xan, the presence of Hem inhibited a combined EPS-electrolyte effect (Figure S2 - 3 a). Hematite exhibits a high density of OH-groups with a strong affinity for carboxyl groups (Gu et al., 1996, 1995; Philippe and Schaumann, 2014), which favors a flat adsorption of EPS onto hematite by multidentate or ring structure interactions, especially at low pH and low surface loading (Gu et al., 1995; Han et al., 2020). Consequently, EPS-Hem interactions outcompete those with multivalent electrolyte cations. In absence of hematite (i.e. Fe-OH groups), overall less sorption sites with a lower affinity for NOM remain (i.e. Al- & Si-OH on illite & quartz) (Meier et al., 1999; Tombácz et al., 2004; Vázquez-Ortega et al., 2014). A higher EPS load on illite Al-OH and adsorption to low-affinity sites (e.g. Si-basal planes, via cation bridging (Newcomb et al., 2017)) favors a shift towards monodentate sorption (Han et al., 2020). Sorbed molecules are thus extended, with functional groups available for multivalent cation induced flocculation.

Finally, the sequence of addition (Figure S2 - 4 a), and Ill:Qua ratios were varied (Figure S2 - 4 b). When added in the end, even Alg and Xan (9 $\%_{wt}$C) allowed some flocculation, but they stabilized the SPM components when added before the minerals, indicating that charge-neutralization driven agglomeration comes to a halt when surfaces are coated by Alg or Xan. Tryp and Glu reacted least sensitive to changes in the sequence of addition, while Pull again showed the highest variability. Furthermore, Tryp, Glu, and Pull were insensitive to variations in the Ill:Qua ratio (Figure S2 - 4 b). Chla and Xan, in turn exhibited a wide polydispersity.

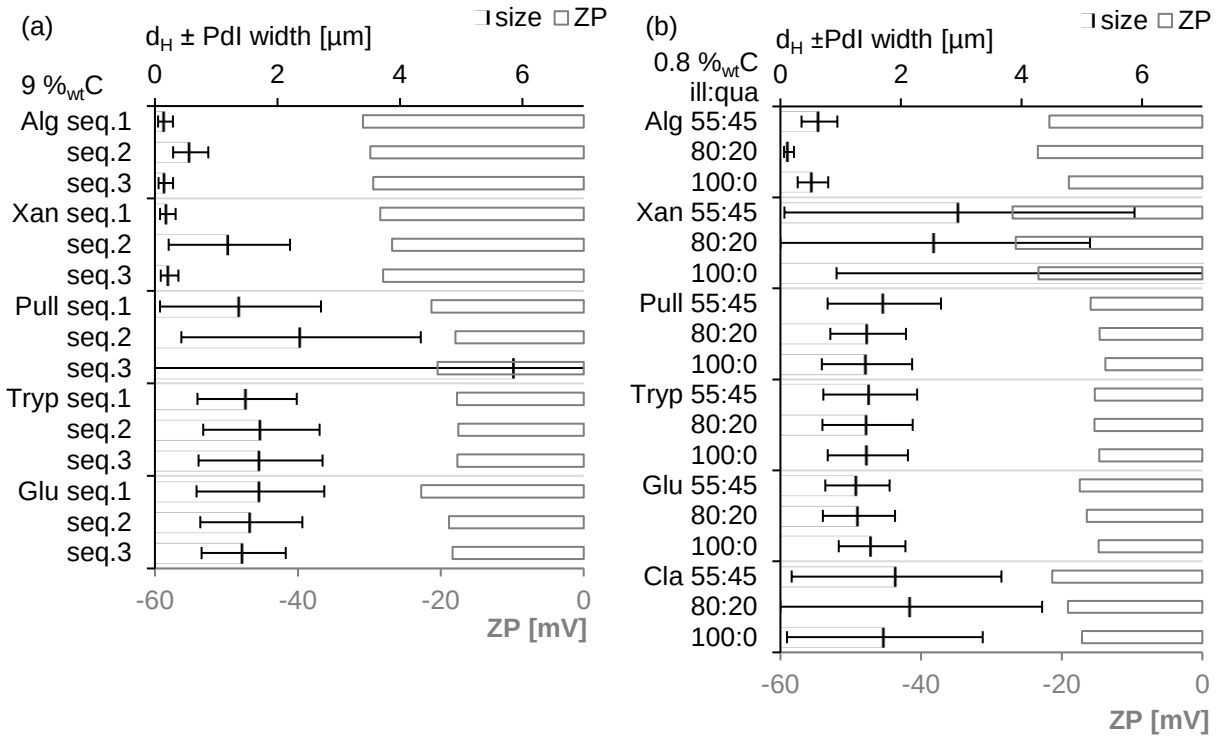

Figure S2 - 4. SPM floc size and ZP with 7 $\%_{wt}$ Hem in 0.1 mM electrolytes, when **(a)** varying sequence of addition at Ill:Qua 55:45 and 9 $\%_{wtC}$ EPS (seq. 1: EPS-Qua-Ill-Hem-electrolytes, seq. 2: Qua-Ill-Hem-electrolytes-EPS, seq. 3: electrolytes-EPS-Qua-Ill-Hem); or **(b)** varying Ill:Qua ratios (55:45, 80:20, 100:0) with 0.8 $\%_{wt}$C EPS, seq. 2.

Summing up, in the presence of Tryp and Glu, SPM analogue floc size was most robust to changes in the sequence of component addition, the Ill:Qua ratio and the EPS proxy concentration. The addition of these low-MW and charge-heterogeneous protein-like substances limited the charge-driven agglomeration of illite and quartz by hematite without stabilizing the single components and narrowed the polydispersity of SPM analogues. Pull also allowed flocculation, floc size was however more sensitive to changes in Pull concentration and component-addition sequence. Xan and Alg, due to their high (negatively charged) carboxyl-group density, mainly induced SPM component stabilization and hindered flocculation. Consequently, Tryp was chosen

as EPS proxy, being the simpler (in terms of molecular structure) and cheaper component compared to Glu. Even though SPM analogues with Tryp were not sensitive to changes in addition sequence, the sequence was set to Qua-Ill-Hem-Tryp-electrolytes, based on the observations with Alg & Xan, which only allowed for agglomeration to occur when EPS was added after the minerals.

S3 – SPM Analogue Component Preparation and Characterization

A) Illite Suspension Preparation. Illite (IMt-2, Silver Hill, MT, USA) rock chips were supplied from the clay minerals society. After milling (30 s, frequency 30 s^{-1}, in 25 mL WC cups with 2 × 15 mm balls, MM 400, Retsch), the coarse fraction was removed by three (re)suspension and settling (5 min) cycles in ultrapure water at a 1:6 clay-solution ratio: After each settling phase, the turbid supernatant was decanted. Collected supernatants were combined and centrifuged for 6 h (5907 g, Cryofuge 6000i, Heraeus). The subsequent two cycles of cation-exchange comprised the following steps: removal of ~ 80 % of the supernatant by slow suction from the top, refill with 0.2 M NaCl, overnight-equilibration on an overhead shaker (16 rpm, Reax 20, Heidolph), and 25 min centrifugation (as above). In the following two cycles ~80 % of the supernatant were replaced by ultrapure water, shaken overnight, and centrifugation for 7 h. These washing cycles were then repeated without overnight-shaking until the supernatant reached an electric conductivity of < 8 µS cm^{-1}. Subsequently, the particle size distribution was narrowed by removing and discarding ~80 % of the supernatant after centrifugation for 32 min during the three following resuspension cycles and finally recovering the supernatant after centrifugation for 6 min in one last resuspension cycle. Centrifugation times were based on equivalent spherical diameter cutoffs of 150 & 350 nm, calculated for illite (density 2.2 g cm^{-3}). The final electric conductivity and pH of four clay suspension preparations were 3 ± 0.3 µS cm^{-1} and 8.9 ± 0.13, respectively. Mass concentrations were determined gravimetrically, vacuum-filtering 3 × 2 mL of suspension by dripping it onto flushed (10 mL ultrapure water), oven-dried (55°C) filters (0.1 µm, PVDF, Durapore, Merck Millipore).

B) Hematite Suspension Preparation. $FeCl_3$ (98 % purity, ACROS Organics) solution was prepared, filtered (, EO-sterilized, GF+CA 0.2 µm syringe filters, Minisart, Sartorius), and spiked into boiling dilute HCl (Primar Plus, trace metal grade, Fisher Chemical), to reach final concentrations of 7.5 mM $FeCl_3$ and 2 mM HCl. For that, 99 mL dilute HCl were brought to boil in closed 250 mL PTFE bottles in the oven at 105°C before spiking 1 mL of $FeCl_3$ solution under vigorous swirling. The bottles were closed again and left in the oven at 105°C, for slow crystallization over 48 h. The lid was tightly but not firmly closed to allow pressure relief but avoid evaporation. When cooled down, the suspension was dialyzed (regenerated cellulose dialysis tubes, cut-off 3.5 kDa, preconditioned for *sensitive assay*, Fisherbrand) against ultrapure water to an electric conductivity > 0.85 and < 1 µS cm^{-1}, yielding a stable suspension for at least 6 month (Figure S3 - 1). Mass concentrations were determined gravimetrically, vacuum-filtering 3 × 2 mL of suspension by dripping it onto pre-weighed filters (0.02 µm, Ø 25 mm, Anodisc, Whatman), oven-drying (55°C), and reweighing the filters.

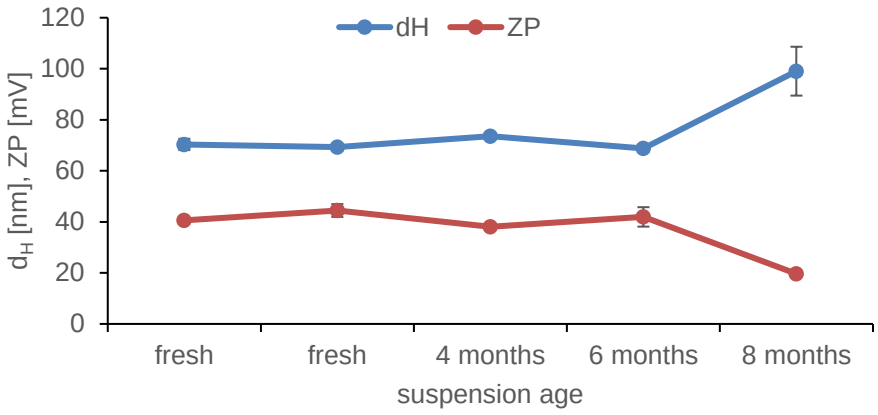

Figure S3 - 1. Stability of hematite stock suspensions regarding hydrodynamic diameter (d_H) and zeta potential (ZP).

C) SPM Components Characterization. Hydrodynamic diameters (d_H), polydispersity indices (PdI), zeta potentials (ZP) and isoelectric points (IEP) were determined by means of dynamic and electrophoretic light scattering (λ 633 nm, Zetasizer Nano ZS, Malvern), employing refractive indices of 1.575 (illite), 3.08 (hematite), and 1.536 (quartz). Size was determined at a backscattering angle of 173°, employing the cumulant method for the autocorrelation function fit. A size measurement consisted of three 15-second runs, and samples were measured at least three times. ZP was measured at a scattering angle of 17° based on the principles of laser Doppler velocimetry: M3-PALS (phase analysis light scattering) is applied to determine the particles' electrophoretic mobility and ZP was calculated from Henry's equation using the Smoluchowski approximation. Each ZP measurement consisted of 20 runs of 3 s. For IEP determinations, pH-titrations (duplicates for Qua & Ill; triplicates for Hem) accompanied by ZP measurements were conducted in different hydrochemical backgrounds (see main text 2.1.), at particle concentrations of 150, 183 and 25 ppm for quartz, illite and hematite, respectively. Shape and additional size information was retrieved from scanning electron microscopy (SEM) imaging (10 kV, spot 3.5, WD 10 mm, ETD detector, Quanta 3D FEG, FEI), for which diluted suspensions were deposited onto 0.02 µm filters (Ø 25 mm, Anodisc, Whatman) by vacuum filtration, oven-dried (55°C), and carbon coated (EM SCD 500, Leica).

As characterization data shows (Table S3 - 1), SPM mineral component suspension preparations were highly reproducible regarding their d_H, PdI and ZP. SEM confirmed the hydrodynamic size of quartz and hematite, while illite's morphology is not well described by d_H (being an equivalent spherical diameter). SEM images (see main text Figure 4) revealed typical thin, irregularly shaped illite platelets with an aspect ratio (AR) of about 1.8. Hematite formed the expected tiny cubes (Wang et al., 2008), and quartz was spherical.

Table S3 - 1. SPM analogue components characterization data.

Stock (pre-parations)	Concentr. [g L^{-1}] [a)]	ZP [mV] [a), b)]	z-ave. d_H [nm] [a)]	PdI [a)]	Shape (SEM)	Size (SEM) [nm] [c)]
Illite (n = 4)	1.56 ± 0.2	-42 ± 3	330 ± 13	0.13 ± 0.01	platelet	l: 495 ± 224 s: 273 ± 99 AR[d)] = 1.8 2 (n = 60)
Hematite (n = 4)	0.56 ± 0.03	+41 ± 3	70.5 ± 2.2	0.15 ± 0.02	cube	a: 76 ± 14 (n = 24)
Quartz (n = 3)	1.5 (weighed)	-60 ± 4	508 ± 20	0.13 ± 0.08	sphere	d: 461 ± 37 (n = 27)

[a)] data represent mean ± standard deviation among different stock preparations

[b)] at natural pH in 1:10 diluted stocks

[c)] data represent median ± X nm to represent the middle 70 % of the measured particles (n)

[d)] AR… aspect ratio: longest (l) to shortest (s) median extension measured

The IEP titrations at different electrolyte or SR-NOM concentrations are given in Figure S3 - 2.

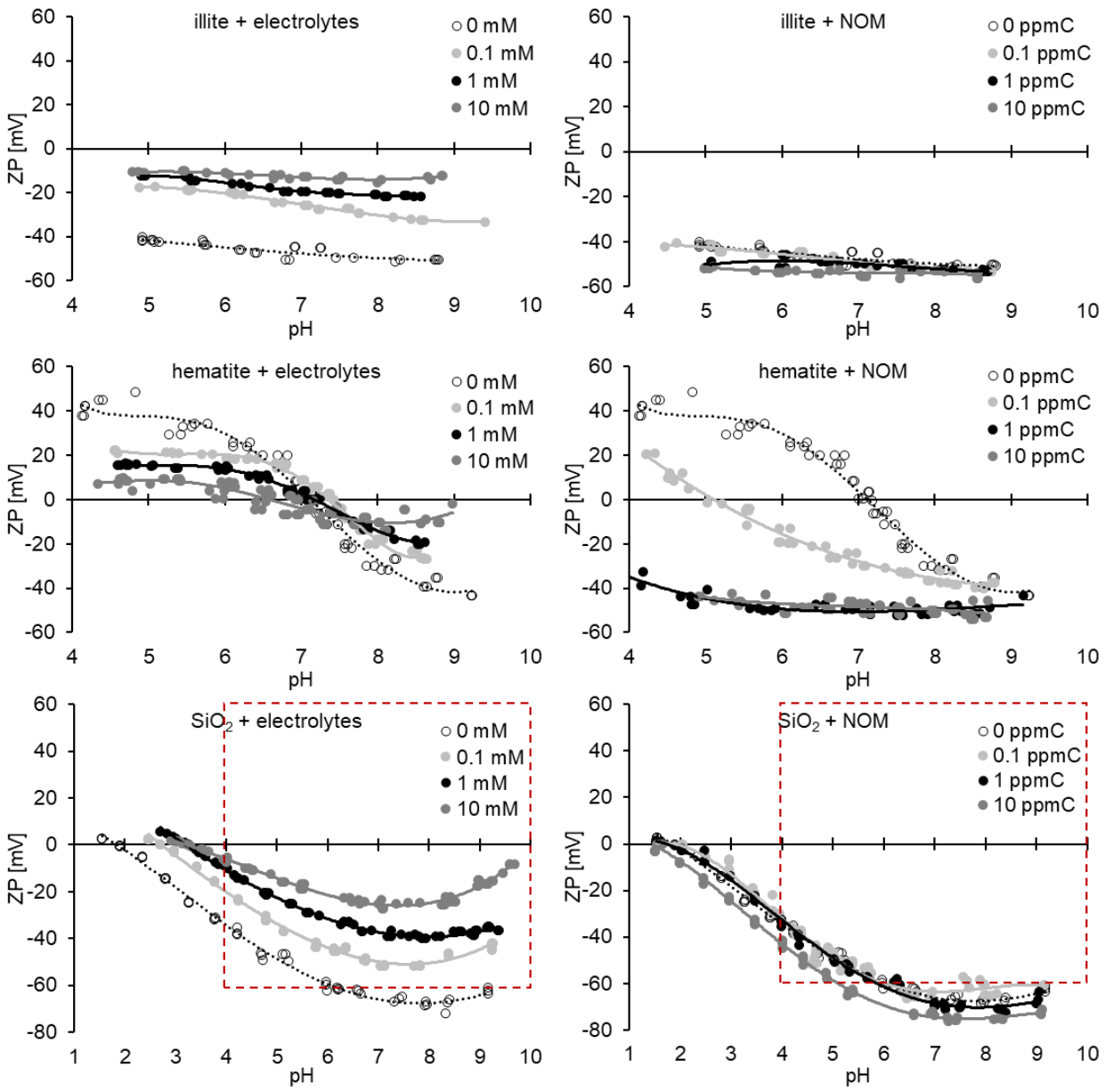

Figure S3 - 2. ZP titration curves of illite (183 ppm), hematite (25 ppm) and quartz (150 ppm) at different electrolyte or SR-NOM concentrations (note the different axis scale for SiO_2; the red frame indicates the range displayed on the other graphs).

Illite and quartz exhibited a negative ZP across all SR-NOM and electrolyte concentrations. Electrolytes reduced the negativity of both minerals and shifted the IEP of quartz from pH 1.82

(0 mM), to 2.71 (0.1 mM) and 3.22 (1 & 10 mM), indicating a non-specific interaction with Ca^{2+} and Mg^{2+}. These values are in accordance with IEPs in literature ranging from 1.5 to 4.5 (mostly <3.5) (Kosmulski, 2001). Illite does not reach an IEP due to its permanent structural charge, which also masks the electrokinetic behavior of edge hydroxyl groups, however, a slight increase in ZP with decreasing pH at low electrolyte concentrations indicates hydroxyl-group protonation. At 10 mM electrolytes, the ZP becomes independent of pH, as cation adsorption to hydroxyl groups outcompetes protonation. The IEP of montmorillonite edges was reported at pH 4 - 5.3 (Pecini and Avena, 2013), which is in line with illite's 0.1 - 10 mM electrolyte titration curves trending towards convergence in that pH range. The strong compensation of negative charge by the addition of electrolytes, suggests cations to also interact with illite basal planes. Indeed, adsorption of (hydrated) Ca^{2+} was suggested to occur on silica basal planes of clay mineral surfaces, acting as Lewis bases in that case (Konan et al., 2007). For (Na-exchanged) illite, the exchange of interlayer Na^{+} by Ca^{2+} (Preocanin et al., 2016) may also play a role in the reduction of negative charge. SR-NOM addition, in turn, slightly increased the negativity of illite at low pH from a ZP of about -40 to -60 mV. This is due to the high density of negatively charged carboxylic groups ($pK_a \sim 3$) on SR-NOM (IHSS, 2020; Ratpukdi et al., 2009), which undergo ligand exchange with clay edge hydroxyl groups favored by low pH (Philippe and Schaumann, 2014). The IEPs of quartz are also slightly lowered (to 1.2 - 1.6) by highly negative SR-NOM.

As expected, hematite constitutes the only (potentially) positively charged mineral component, at least at acidic up to neutral pH. Positivity as well as IEPs (pH 7.4, 7.2, 6.6) decrease with increasing electrolyte concentrations, and their common interception point is located at pH 7.6 ± 0.08. The negative shift of the interception point to -7.9 ± 1.2 mV indicates adsorption of SO_4^{2-} (Walsch and Dultz, 2010). All IEP values are within the typical range for hematite

(Kosmulski, 2001). The presence of SR-NOM completely reversed its charge (to about -40 mV), as explained by adsorption due to the strong interactions of hydroxyl groups on FeOx with carboxyl groups of NOM (Gu et al., 1995; Vindedahl et al., 2016). Association of NOM coatings with FeOx was observed on natural SPM (Poulton and Raiswell, 2005) and in the lab (Baalousha et al., 2008). Only at the lowest concentration (0.1 ppmC) the surface was probably not completely covered by NOM, as no full charge reversal occurred, but the IEP was shifted down to pH 5.2. This was also observed by (Baalousha, 2009) and is in accordance with the observation that agglomeration in the presence of NOM peaked at pH 4 - 5 at similar NOM:FeOx concentration ratios (Baalousha et al., 2008).

S4 – SPM Analogue Generation

A) Mastersizer "Freefall" Stirred-Batch Setup. The setup consisted of two stirred batch reactors (i.e., 1 L Duran borosilicate glass beakers and Heidolph RZR1 stirres with Bochem 7×7 cm 6-hole blades, operated at 100 rpm), with one batch being elevated relative to the other (Figure S4 - 1). Connecting tubes (d_i = 6.4 mm, Tygon E-3603, Saint-Gobain) to and from the laser diffractometer (Mastersizer 2000, Malvern) were kept as short as possible. To minimize floc disturbance during sample introduction, the sample was passed in freefall through the measurement cell at a flow of ~ 6 mL s^{-1}, adjusted by a hose clamp located on the cell inflow tube. A peristaltic pump (520U, Watson Marlow) connected by PVC tubing (d_i = 16 mm, length = 1 m) was operated at the same flow to close the circuit and keep the batch fill-levels stable at 750 mL per batch (with a total sample volume of 1.6 L in the system including measurement cell and tubes).

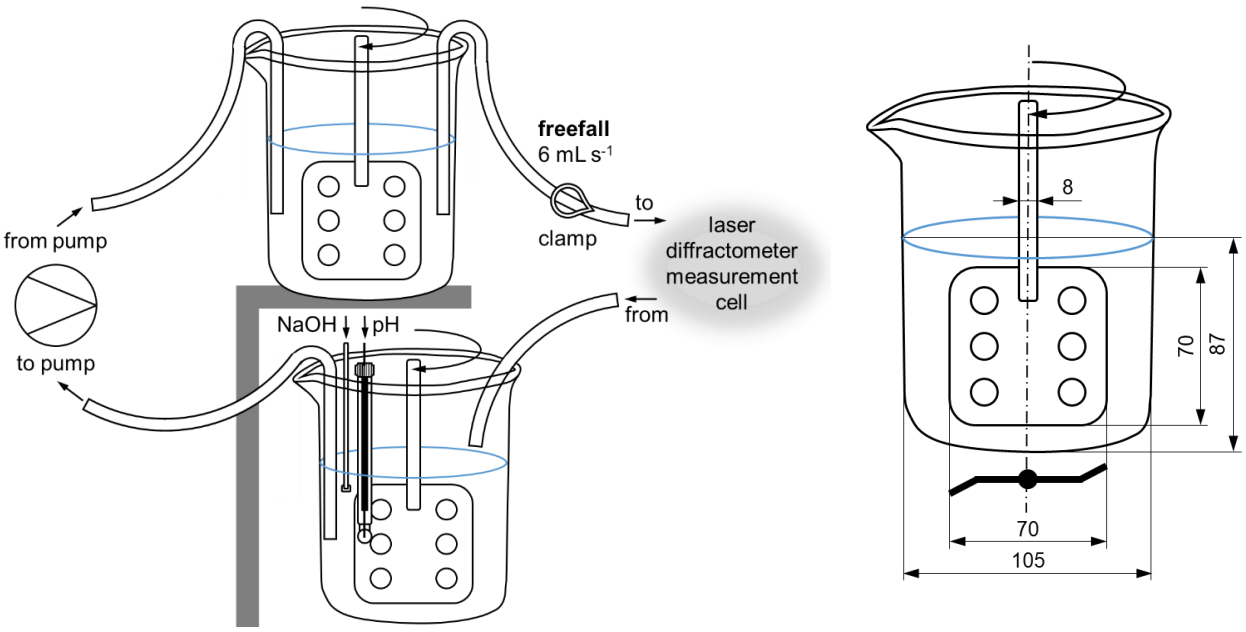

Figure S4 - 1. Freefall Mastersizer setup and batch dimensions.

B) SPM Composition Refinement. For SPM analogue composition refinement in the described Mastersizer setup, the *association procedure* (see main text 2.3) was employed at pH 5 and 0.1 mM electrolytes. To tune hematite concentrations, SPM mixtures were prepared at increasing hematite concentrations of 0, 2, 5, 7 $\%_{wt}$ of the total mineral mass (Figure S4 - 2). Floc association was quicker at higher hematite concentrations, confirming charge neutralization by hematite addition, as suggested in S2. As mixtures with 5 and 7 % Hem quickly assembled to a plateau size, they were further investigated with varying Tryp concentrations.

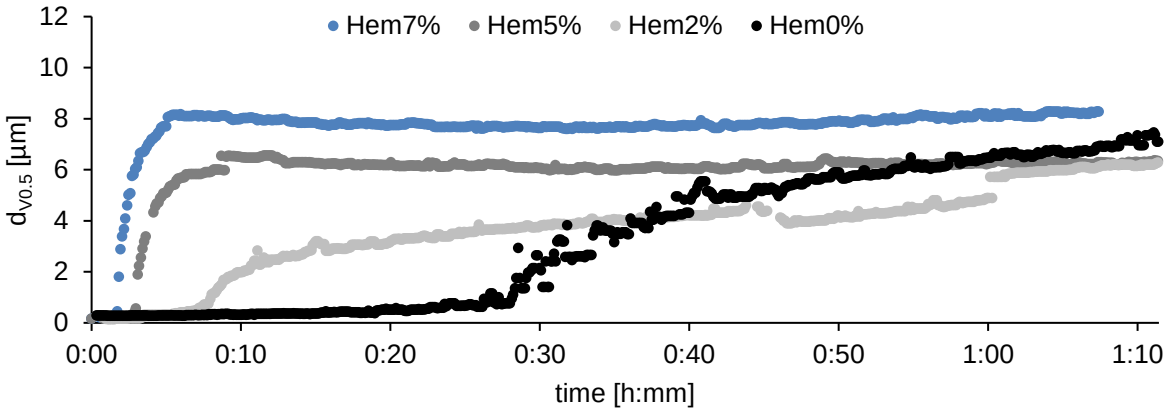

Figure S4 - 2. SPM association at different Hem concentrations (0, 2, 5, 7 $\%_{wt}$) at Ill:Qua 55:45, with 5 $\%_{wt}$C Tryp in 0.1 mM electrolytes; sequence of addition Qua-Ill-Hem-Tryp-electrolytes.

C-based Tryp concentrations of 5 and 10 $\%_{wt}$ were tested (Figure S4 - 3). At 7 $\%_{wt}$ Hem, size plateaued for at least 1 h irrespective of Tryp concentrations. At 5 $\%_{wt}$ Hem with 10 $\%_{wt}$ Tryp, the plateau was not stable beyond 40 min. Hence, a mix of 7 $\%_{wt}$ Hem and 5 $\%_{wt}$ Tryp was selected.

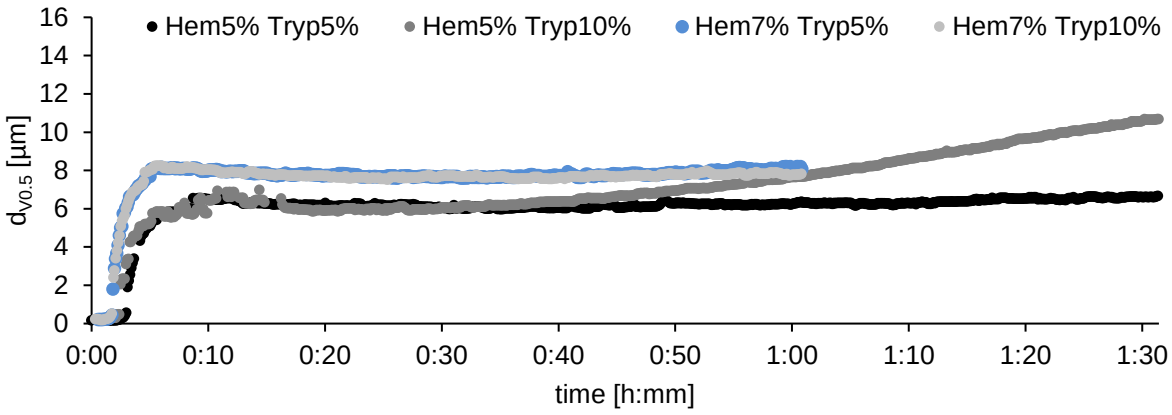

Figure S4 - 3. SPM association at Ill:Qua 55:45 in 0.1 mM electrolytes with 5 or 7 $\%_{wt}$ Hem and 5 or 10 $\%_{wt}$ Tryp.

Varying the illite-to-quartz ratio in that mix had only little effect (Figure S4 - 4), confirming screening tests (S2). The ratio of 55:45 generated a slightly more even plateau size and was thus selected for SPM analogue generation. With 7 $\%_{wt}$ Hem, the Ill:Qua ratio of 55:45 translates to 41.85 $\%_{wt}$ quartz and 51.15 $\%_{wt}$ illite in the total mineral fraction (given in main Text Table 1).

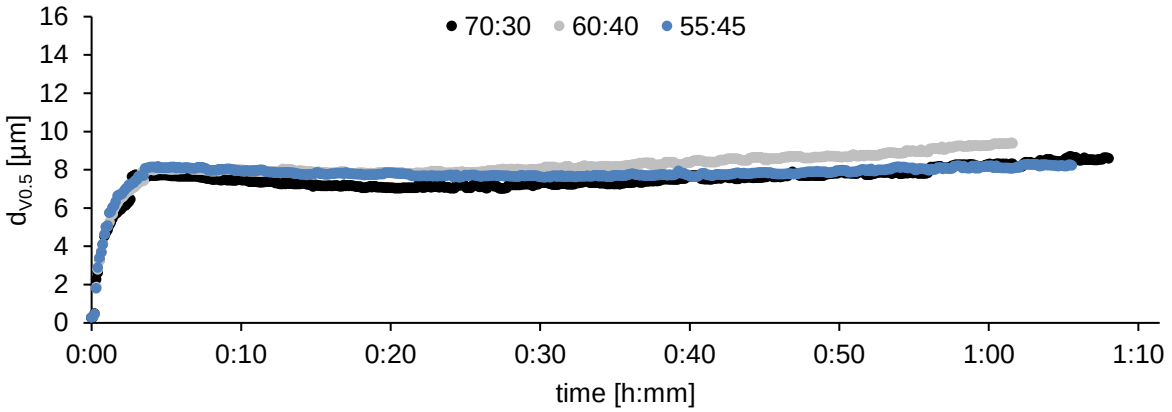

Figure S4 - 4. SPM association at decreasing Ill:Qua ratios, with 7 $\%_{wt}$ Hem and 5 $\%_{wt}$ Tryp.

C) SPM Analogue Preparation Procedure. A recipe for SPM analogue preparation is given in Table S4 - 1. Stock dilutions in 100 mL acidified ultrapure water (pH 5) were prepared right before mixing the components to minimize losses to the vessels (especially for hematite). For SPM assemblage, stirred batches were filled with 0.4-0.6 L acidified ultrapure water (depending on whether electrolytes and/or SR-NOM were included), and quartz and illite were directly spiked from stocks. Dilutions of hematite, tryptophan, and facultatively electrolytes and/or SR-NOM were quickly added to both stirred batches simultaneously in the listed sequence.

Table S4 - 1. SPM analogue preparation from component stock suspensions.

Components (addition sequence)	**Volume [L] of dilution** [a)]	**Conc. Unit**	**Conc. in dilutions**	**Conc. final**
Quartz	0.4 - 0.6 [b)]	mg L^{-1}	25.1 - 37.7 [b)]	18.83
and Illite		mg L^{-1}	30.7 - 46.0 [b)]	23.02
Hematite	0.1	mg L^{-1}	25.2	3.15
Tryptophan	0.1	mg C L^{-1}	18	2.25
Electrolytes [c)]	0.1	mM	1.6 - 160	0.1 - 10
SR-NOM [c)]	0.1	mg C L^{-1}	1.6 - 160	0.1 - 10
final Volume [L]	0.8			

[a)] prepared in acidified ultrapure water (~pH 5) right before SPM generation

[b)] depending on whether facultative components are added

[c)] facultatively added

S5 – SPM Analogue Protocol Validation

A) Rationale Beyond Selected Hydrochemistry for Protocol Validation. Based on the properties of the selected SPM analogue components (see S1 and S3-C), the hydrochemical conditions employed for protocol validation (i.e., pH 5, no SR-NOM addition, 0.1 mM electrolytes) should allow floc formation. A pH of 5 assures the positive surface charge of hematite and was convenient as it remained stable without any readjustments necessary. SR-NOM was excluded, as it has a high density of negatively charged carboxyl groups and a high potential to stabilize SPM components, masking their intrinsic surface properties. Similarly, high electrolyte concentrations approaching or exceeding the critical coagulation concentration, mask the relevance of component's surface characteristics for flocculation. Hence, the lowest electrolyte concentration within the range suggested by OECD TG 318 (see main text 2.1) was used.

B) Determination of SPM Floc Size and Fractal Dimension. To investigate the temporal evolution of floc size and fractal dimension, angular light scattering patterns were recorded every 6 - 7 s (measurement duration 0.5 s) by laser diffractometry (Mastersizer 2000, Malvern). Background correction measurements were conducted in deionized water (measurement duration 30 s). Size measures were retrieved based on Mie theory, employing the general purpose analysis mode and a refractive index of 1.544. Volume-based median diameters ($d_{V0.5}$) denote the floc diameter which 50 % of the sample volume exceed and 50 % of the sample volume fall below. To plot the temporal evolution of floc size, recorded $d_{V0.5}$ data were smoothed calculating moving medians over 7 subsequent data points (covering ~ 40 s measurement time). Volume-based size distributions were plotted as medians of 10 subsequent data records (covering ~ 60 s measurement

time). The same is true for volume-based mode diameters (mode d_V) which denote the peak-diameter of the largest peak in the volume-based size distribution.

The fractal dimension (D_f) was determined according to literature (Bushell and Amal, 2000; Thill et al., 2000). It describes the structural compactness of an agglomerate via the proportional relation ($m \propto r^{Df}$) of mass (m) and agglomerate size (r) and takes values between 1 and 3. For time resolved fractal dimension plots, at each plotted time point, the median angular scattering intensities of 7 subsequent recorded scattering patterns (covering ~40 s) were extracted. The scattering angles in air were corrected by the refractive index (RI) of water (1.33) to get the scattering angles in water (i.e., the sample matrix) (Equation S5 - 1).

$$angle_{water} = arcsin\left(\frac{sin(angle_{air})}{RI_{water}}\right)$$

Equation S5 - 1. Correction of scattering angle with refractive index of water.

The intensities were corrected for detector areas and nonlinearity employing instrument specific correction factors for each detector/angle provided by Malvern Panalytical (Worchestershire, UK).

According to Equation S5 - 2, the fractal scattering regime is characterized by a power law decrease of the scattered light intensity (I) with increasing scattering angle (expressed as the scattering wave vector (q)) by the power of the fractal dimension (D_f). Hence, a log-log plot of the scattering intensities versus detection angles reveals the fractal range as a linear negative correlation (Bushell et al., 2002a).

$$I(q) \propto q^{-D_f}$$

Equation S5 - 2. Correction of scattering angle with refractive index of water.

Figure S5 - 1 shows an example for the development of the fractal regime during SPM analogue association over time. Starting from a primary particle scattering dominated pattern at the

beginning of the floc association, the fractal regime was building up until the angular scattering pattern stabilizes concurrently with the plateauing of the floc size. As the SPM flocs are composed of primary particles of different sizes, the non-linear behavior at higher angles (primary particle scattering effect) can be attributed to a structural "dilution effect" of more intensely scattering larger particles (quartz) within the floc. At low angles, transition to Guinier scattering (agglomerate edge effects) can be observed (Bushell et al., 2002b, 1998).

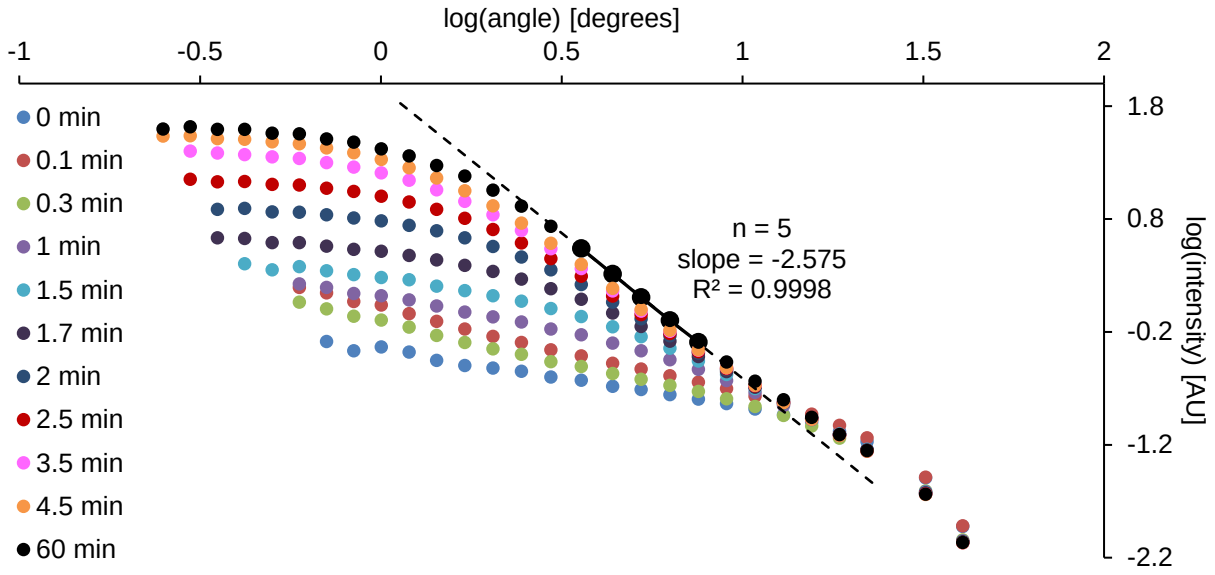

Figure S5 - 1. Time-resolved fractal regime evolution during SPM association (pH 5, 0.1 mM)

To minimize impacts of Guinier (levelling at lower angles) and primary particle scattering (shoulder at higher angles), the fractal linear range was automatically selected by maximizing the slope of 5 points within the fractal regime between log angles 0 and 1.4 (as indicated by the black dashed line in Figure S5 - 1). The slope corresponds to $-D_f$, and R^2 was typically > 0.999.

S6 – Reproducibility and Structure of SPM Analogue Flocs

Figure S6 - 1 shows the reproducibility of SPM analogue floc association employing the same component stock batches (within-batch-reproducibility).

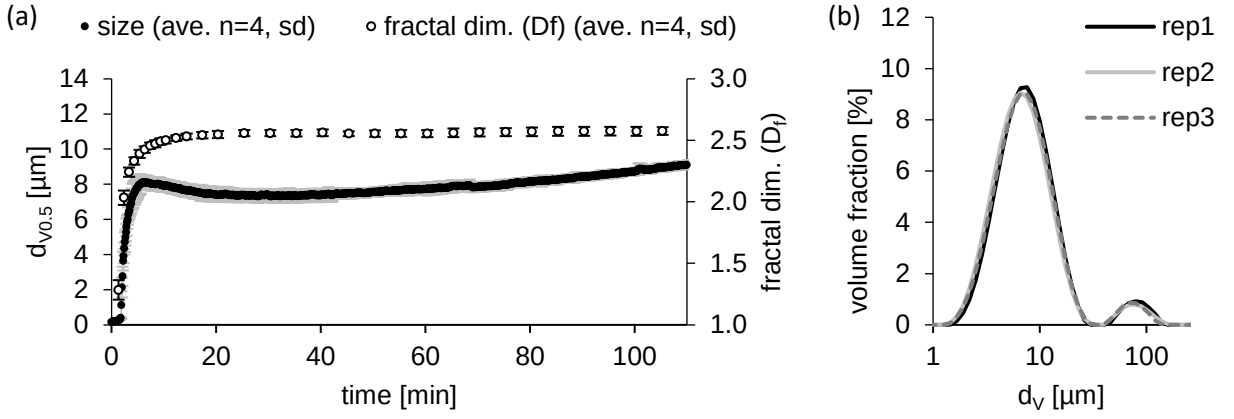

Figure S6 - 1. (a) Evolution of volume-based median floc diameters ($d_{V0.5}$) and fractal dimension (D_f) during floc association (ave. ± sd) of four within-batch replicates (pH 5, 0.1 mM electrolytes); **(b)** respective size distributions at 60 min.

Reproducibility of SPM analogue size distributions by preparation through 24 h *shaker equilibration* is shown in Figure S6 - 2.

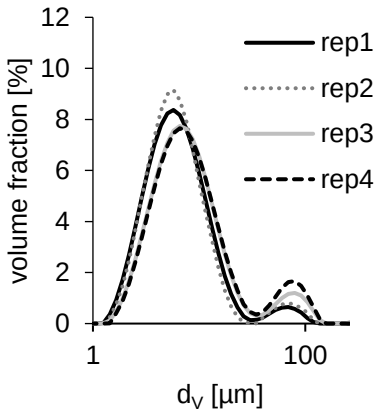

Figure S6 - 2. Within-batch reproducibility (n = 4) of floc size distributions upon preparation by 24 h *shaker equilibration* (comparison after 60 min in the Mastersizer setup)

SEM images of SPM analogues reveal structural details such as hematite particles acting as bridges between illite and quartz (Figure S6 - 3), the distribution of hematite primarily on illite edges (Figure S6 - 4) and quartz mostly located on the floc surface (Figure S6 - 5).

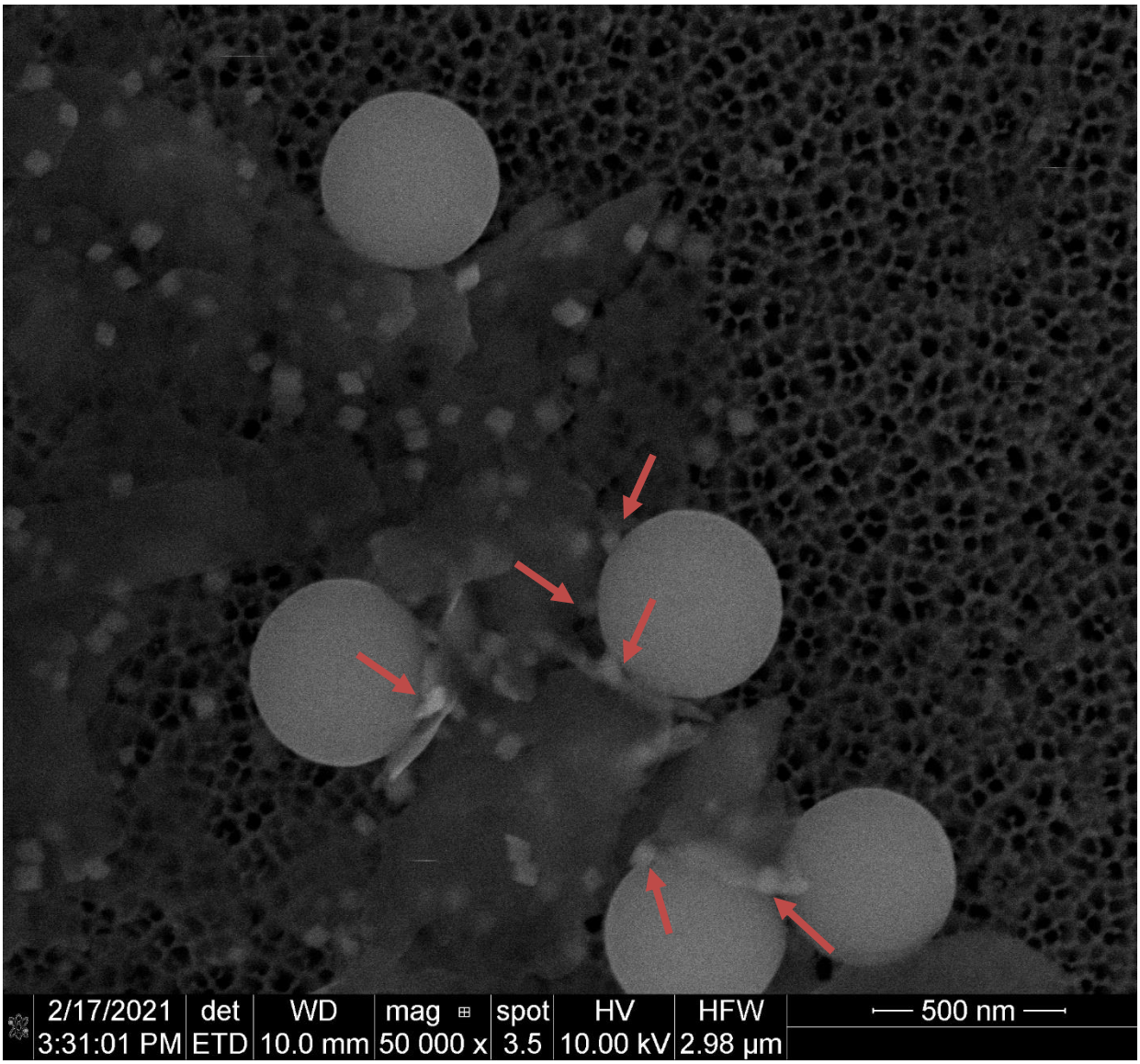

Figure S6 - 3. SEM image showing hematite bridging between illite and quartz.

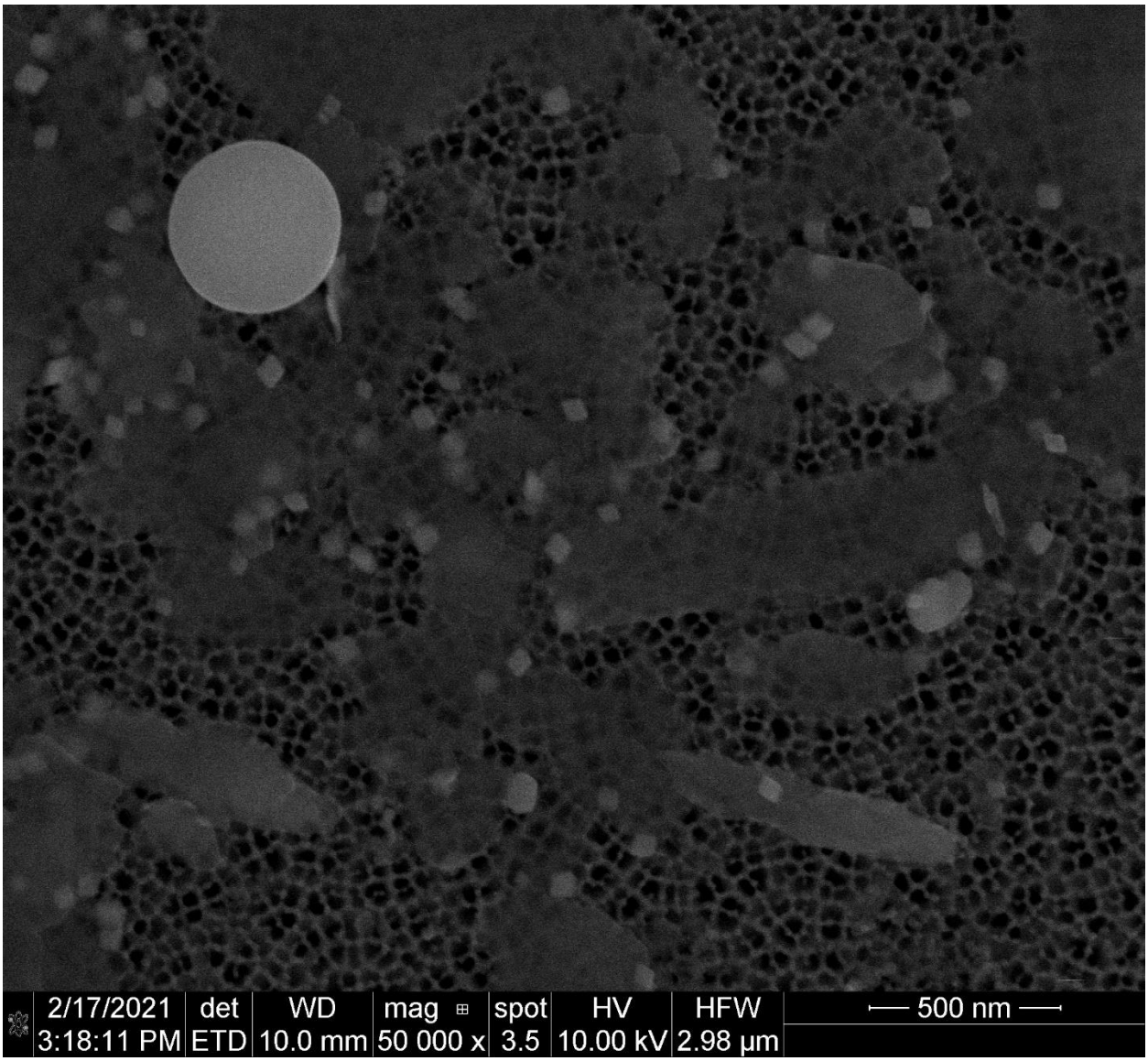

Figure S6 - 4. SEM image showing hematite mostly sitting on illite edges.

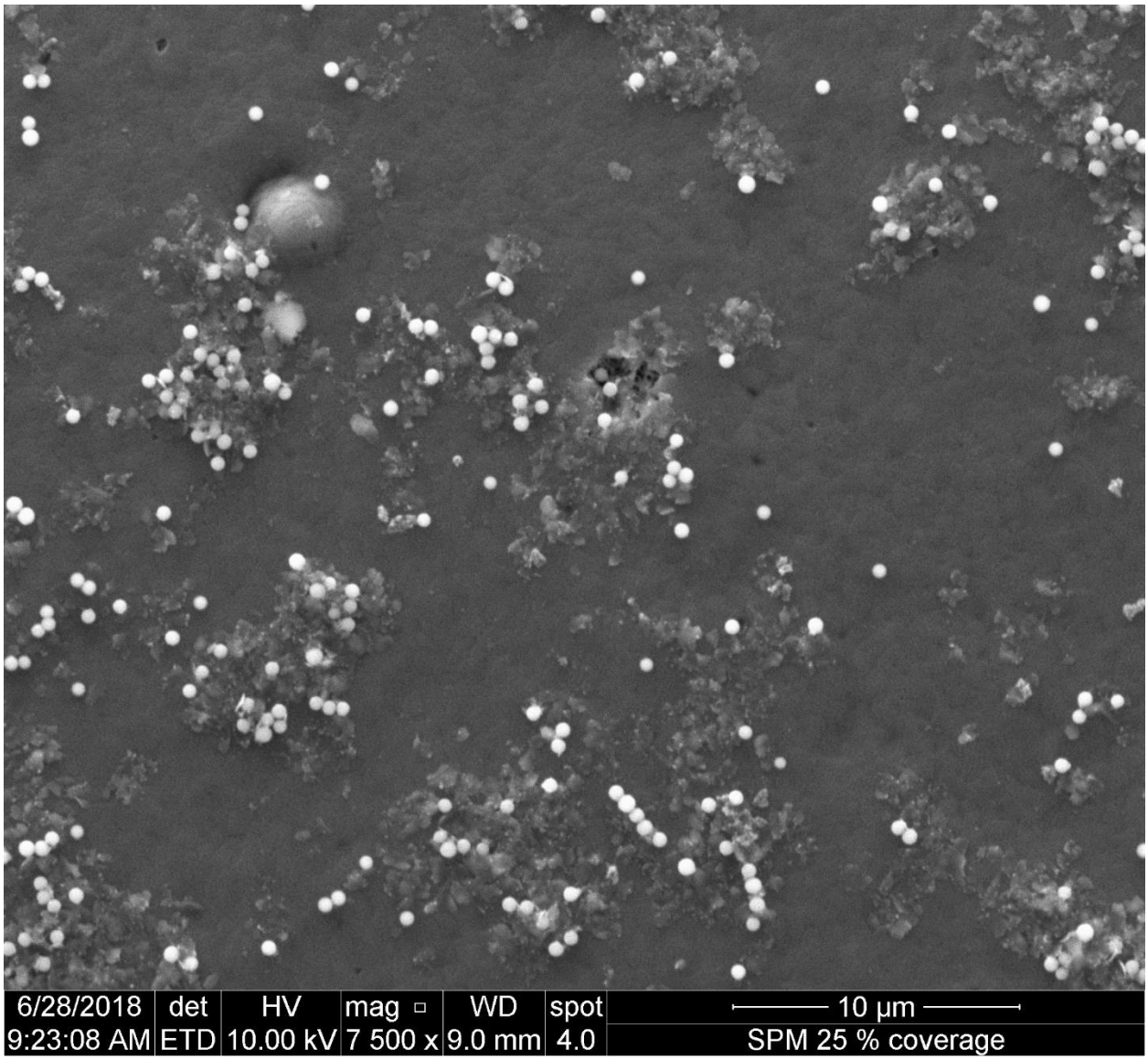

Figure S6 - 5. SEM image showing quartz frequently on the surface of the flocs.

S7 – Floc Size Evolution During SPM Association

During initial SPM association, prevalence of nano-sized primary particles (with quartz being the largest component) results in a dominance of diffusion-driven collisions (Figure S7 - 1 a). With ongoing flocculation and size increase, advective collisions dominate (Figure S7 - 1 b).

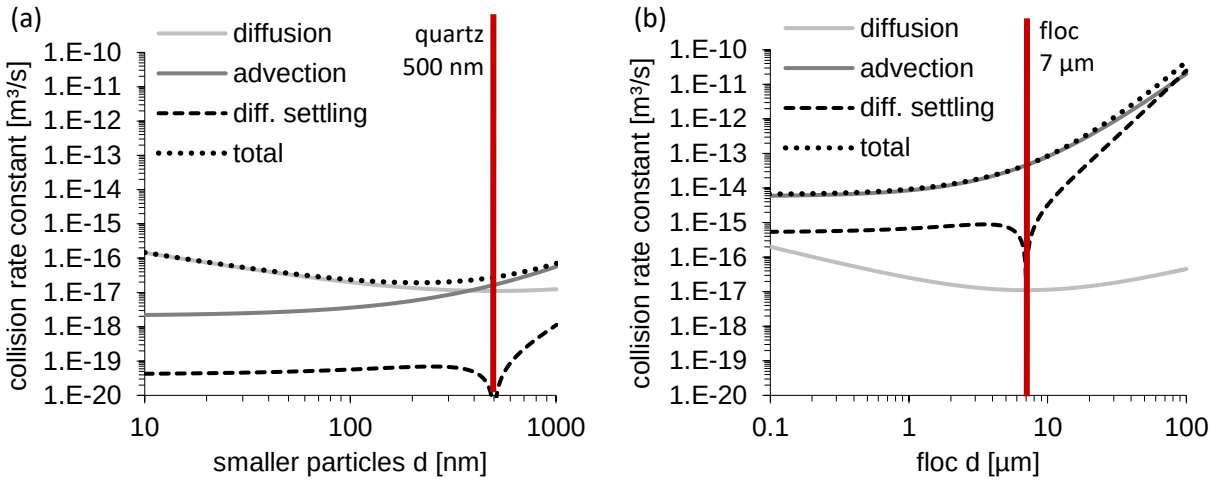

Figure S7 - 1. Smoluchowski-based collision rate constants at T = 21°C and G = 100 s^{-1} **(a)** for 500 nm quartz with smaller (hematite or illite) component particles (assuming an average density of 2.5 g/cm³ for all particles), and **(b)** for plateau-size (7 µm) SPM flocs with smaller & larger flocs, assuming a floc density of 1.5 g/cm³. Model calculations based on Han and Lawler (1992).

A rough calculation of the positive and negative surface area fractions present in the SPM component mix reveals the dominance of negative surfaces, at a ratio of ~10:1 (Table S7 - 1).

Table S7 - 1. Approximation of the positive and negative SPM component surface fraction.

	Mass Fraction [%wt]	Shape	Size (SEM) [nm]	Density [g cm^{-3}]	Surface Fraction [%SA]	Charge at pH 5	Surface Fraction [%SA]
Quartz	41.9	sphere	d = 461	2.0 [c)]	5.6	negative	**92.5**
Illite	51.2	disc	d = 360 [a)]	2.2 [c)]	86.9	negative	
			h = 11 [b)]		5.3	positive	**7.5**
Hematite	7.0	cube	a = 76	5.26 [d)]	2.2	positive	

[a)] median of longest and shortest dimensions of 60 platelets measured on SEM.

[b)] illite thickness by TEM from Beckett *et al.* (1997)

[c)] from MSDS

[d)] bulk material density

The resumption of SPM floc growth after a phase of plateauing size during SPM association (see main text Figure 5 a, 50 rpm curve) coincides with the proliferation of a second peak in the size distribution (Figure S7 - 2) and a slow decrease in the fractal dimension (see main text Figure 5 b, D_f at 50 rpm), indicating secondary floc formation.

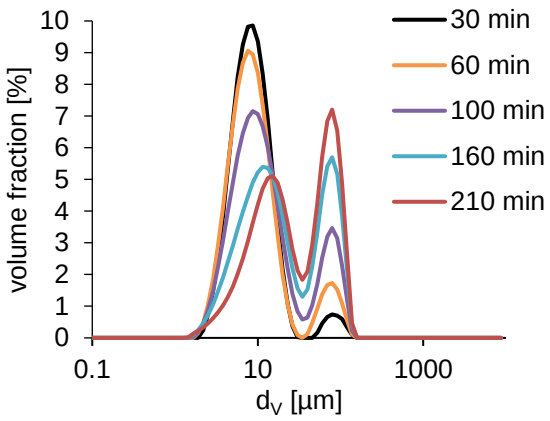

Figure S7 - 2. Temporal evolution of the floc size distribution during association at 50 rpm stirring speed and 45 ppm SPM (mineral concentration), indicating secondary floc formation.

S8 – Resilience of SPM Analogues to Physical and Hydrochemical Impacts.

Figure S8 - 1 shows size distributions of SPM analogues after storage and resuspension by different means. Over a period of min. 8 days, size distributions are resilient to physical impacts.

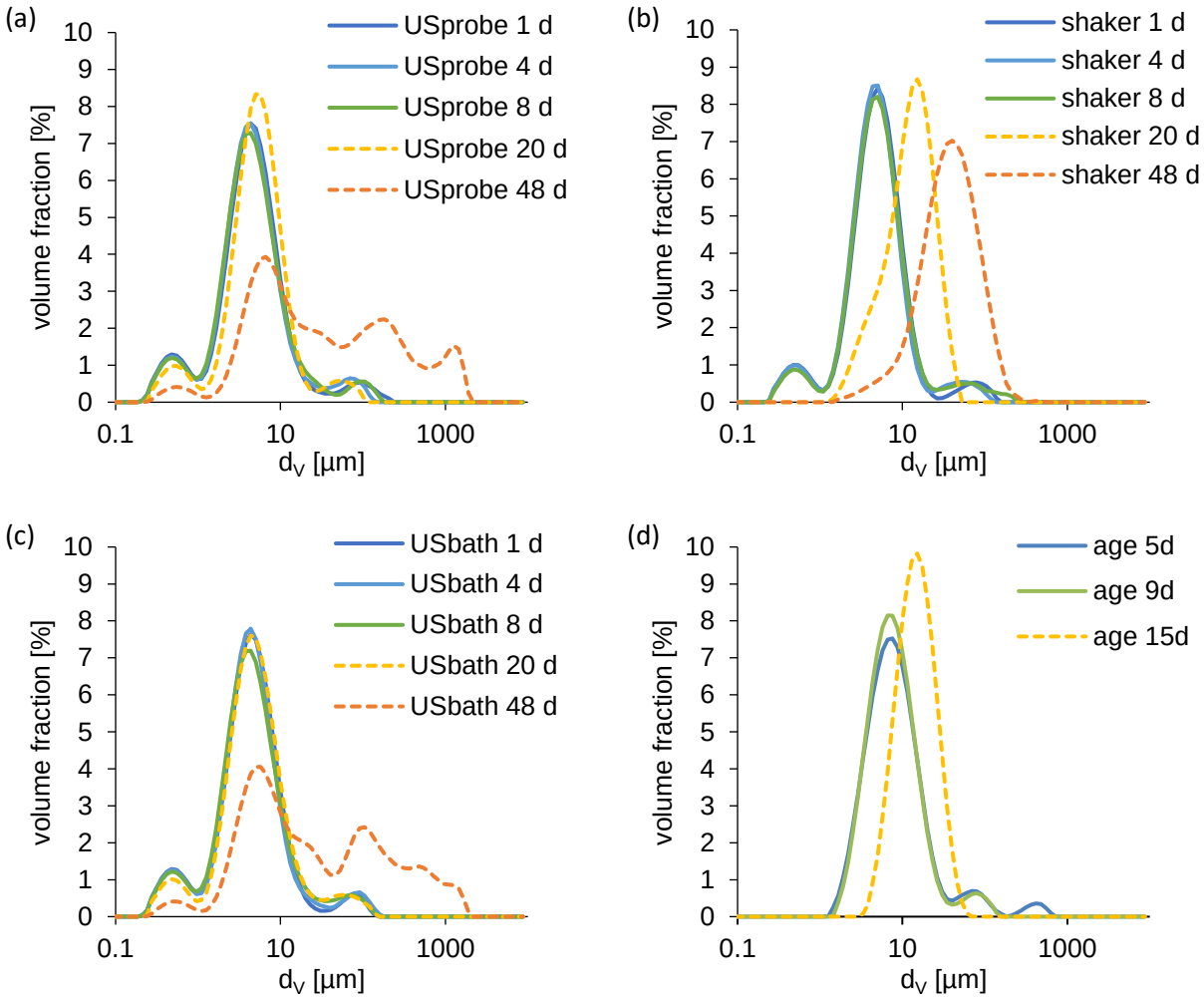

Figure S8 - 1. Floc size distributions (compared after 60 min in the Mastersizer setup) after storage and resuspension of the same three batches at different time intervals by US-probe **(a)**, shaker **(b)**, US-bath **(c)**, respectively; and of three independent batches resuspended by shaking after different storage times each **(d)**.

Association of SPM analogues at halved SPM concentrations (22.5 ppm mineral mass) yielded larger flocs than association at 45 ppm. Upon resuspension differences were less pronounced (Figure S8 - 2 a), and batches prepared at half concentrations as well as batches diluted to half concentrations (either before or after shaking for 24 h) all approached similar sizes, when exposed to controlled stirring conditions in the Mastersizer setup (Figure S8 - 2 b).

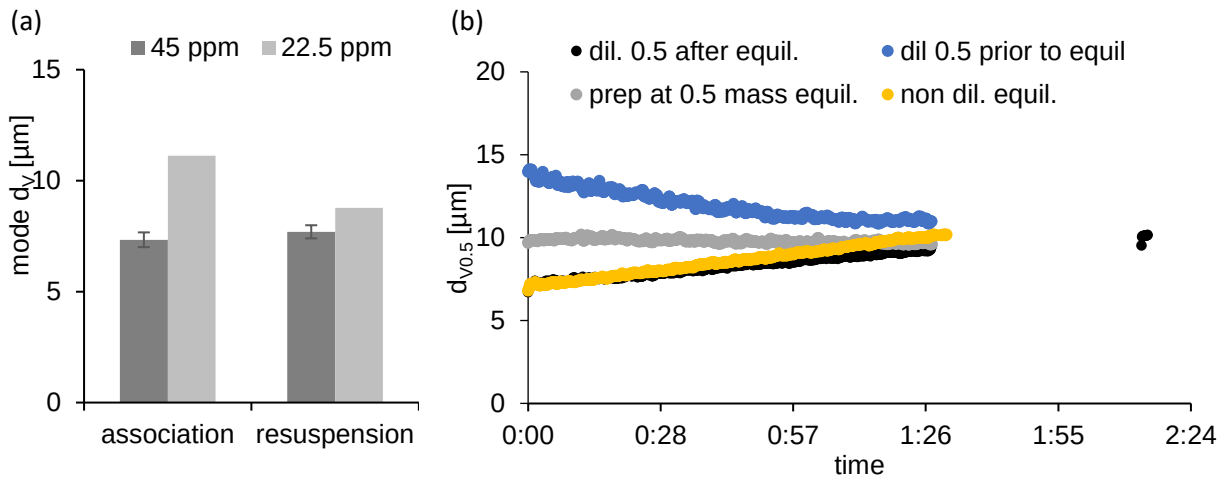

Figure S8 - 2. (a) Size of SPM at concentrations of 45 ppm and 22.5 ppm during the association plateau phase and after resuspension (compared after 60 min measurement time); **(b)** Volume-based median diameter of resuspended, shaker-equilibrated (24 h) SPM: diluted to half mass (before or after shaker-equilibration), prepared at half-mass, or non-diluted (45 ppm).

As Figure S8 - 3 and Figure S8 - 4 show, dilution of SPMzero (prepared by *association* or *shaker equilibration* procedure) to hydrochemical conditions which were unfavorable for floc association (i.e., 0.1 mM electrolytes and 1 ppmC SR-NOM), did not induce disintegration of flocs, not even after storage and resuspension.

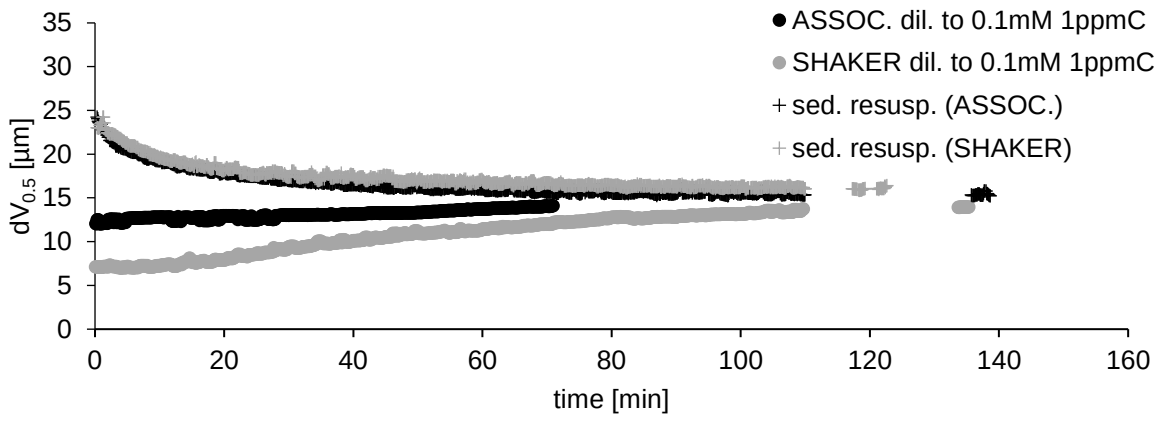

Figure S8 - 3. SPMzero prepared by *association* or *shaker equilibration* procedure and diluted 1:1 to a hydrochemistry of 0.1 mM electrolytes and 1 ppmC SR-NOM compared to the same samples after storage and resuspension.

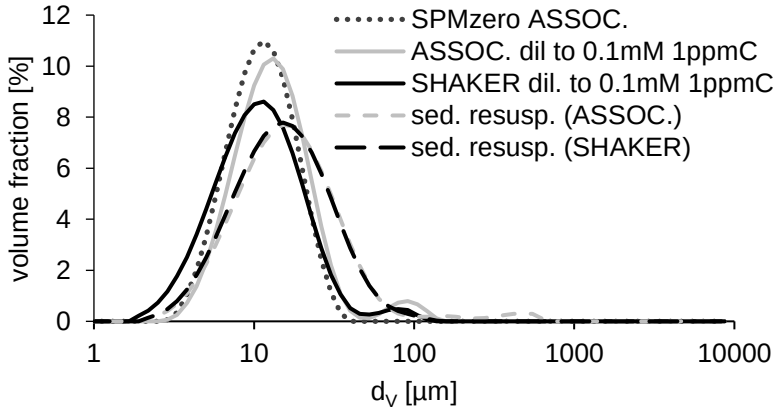

Figure S8 - 4. Size distributions of SPMzero during association, after 1:1 dilution of freshly *associated* and over-night *shaker equilibrated* SPMzero to a hydrochemistry of 0.1 mM electrolytes and 1 ppmC SR-NOM, and after 6d-storage and resuspension of these samples. (Compared after 60 min in the Mastersizer setup.)

References

Abdolahpur Monikh, F., Praetorius, A., Schmid, A., Kozin, P., Meisterjahn, B., Makarova, E., Hofmann, T., von der Kammer, F., 2018. Scientific rationale for the development of an OECD test guideline on engineered nanomaterial stability. NanoImpact 11, 42–50. doi:10.1016/j.impact.2018.01.003

Artemyev, V.E., 1996. Geochemistry of Organic Matter in River-Sea Systems. Springer Netherlands, Dordrecht. doi:10.1007/978-94-009-1681-4

Ates, O., 2015. Systems Biology of Microbial Exopolysaccharides Production. Front. Bioeng. Biotechnol. 3, 1–16. doi:10.3389/fbioe.2015.00200

Baalousha, M., 2016. Effect of nanomaterial and media physicochemical properties on nanomaterial aggregation kinetics. NanoImpact. doi:10.1016/j.jcis.2016.10.037

Baalousha, M., 2009. Aggregation and disaggregation of iron oxide nanoparticles: Influence of particle concentration, pH and natural organic matter. Sci. Total Environ. 407, 2093–2101. doi:10.1016/j.scitotenv.2008.11.022

Baalousha, M., Manciulea, A., Cumberland, S., Kendall, K., Lead, J.R., 2008. Aggregation and Surface Properties of Iron Oxide Nanoparticles: Influence of pH and Natural Organic Matter. Environ. Toxicol. Chem. 27, 1875. doi:10.1897/07-559.1

Bantignies, J., Moulin, C.C. dit, Dexpert, H., 1997. Wettability Contrasts in Kaolinite and Illite Clays: Characterization by Infrared and X-ray Absorption Spectroscopies. Clays Clay Miner. 45, 184–193. doi:10.1346/CCMN.1997.0450206

Beckett, R., Murphy, D., Tadjiki, S., Chittleborough, D.J., Calvin Giddings, J., 1997. Determination of thickness, aspect ratio and size distributions for platey particles using sedimentation field-flow fractionation and electron microscopy. Colloids Surfaces A Physicochem. Eng. Asp. 120, 17–26. doi:10.1016/S0927-7757(96)03716-8

Buffle, J., Wilkinson, K.J., Stoll, S., Filella, M., Zhang, J., 1998. A Generalized Description of Aquatic Colloidal Interactions: The Three-colloidal Component Approach. Environ. Sci. Technol. 32, 2887–2899. doi:10.1021/es980217h

Bushell, G., Amal, R., 2000. Measurement of Fractal Aggregates of Polydisperse Particles Using Small-Angle Light Scattering. J. Colloid Interface Sci. 221, 186–194. doi:10.1006/jcis.1999.6532

Bushell, G., Amal, R., Raper, J., 1998. The Effect of Polydispersity in Primary Particle Size on Measurement of the Fractal Dimension of Aggregates. Part. Part. Syst. Charact. 15, 3–8. doi:10.1002/(SICI)1521-4117(199802)15:1<3::AID-PPSC3>3.0.CO;2-K

Bushell, G., Yan, Y.D., Woodfield, D., Raper, J., Amal, R., 2002a. On techniques for the measurement of the mass fractal dimension of aggregates. Adv. Colloid Interface Sci. 95, 1–50. doi:10.1016/S0001-8686(00)00078-6

Bushell, G., Yan, Y.D., Woodfield, D., Raper, J., Amal, R., 2002b. On techniques for the

measurement of the mass fractal dimension of aggregates. Adv. Colloid Interface Sci. 95, 1–50. doi:10.1016/S0001-8686(00)00078-6

Camesano, T.A., Wilkinson, K.J., 2001. Single molecule study of Xanthan conformation using atomic force microscopy. Biomacromolecules 2, 1184–1191. doi:10.1021/bm015555g

Carnal, F., Clavier, A., Stoll, S., 2015. Modelling the interaction processes between nanoparticles and biomacromolecules of variable hydrophobicity: Monte Carlo simulations. Environ. Sci. Nano 2, 327–339. doi:10.1039/c5en00054h

Cuadros, J., 2017. Clay minerals interaction with microorganisms: a review. Clay Miner. 52, 235–261. doi:10.1180/claymin.2017.052.2.05

Elimelech, M., Gregory, J., Jia, X., Williams, R.A., 1995. Modelling of aggregation processes, in: Particle Deposition & Aggregation. Elsevier, Woburn, pp. 157–202. doi:10.1016/B978-075067024-1/50006-6

Filella, M., 2007. Colloidal Properties of Submicron Particles in Natural Waters, in: Wilkinson, K.J., Lead, J.R. (Eds.), Environmental Colloids and Particles: Behaviour, Separation and Characterisation Edited. Wiley & Sons, West Sussex, pp. 17–63.

Flemming, H.-C., Wingender, J., 2010. The biofilm matrix. Nat. Rev. Microbiol. 8, 623–633. doi:10.1038/nrmicro2415

Grasso, D., Subramaniam, K., Butkus, M., Strevett, K., Bergendahl, J., 2002. A review of non-DLVO interactions in environmental colloidal systems. Rev. Environ. Sci. Biotechnol. 1, 17–38. doi:10.1023/A:1015146710500

Gregory, J., 2005. Particles in Water. CRC Press, Boca Raton. doi:10.1201/9780203508459

Grillo, R., Rosa, A.H., Fraceto, L.F., 2015. Engineered nanoparticles and organic matter: A review of the state-of-the-art. Chemosphere 119, 608–619. doi:10.1016/j.chemosphere.2014.07.049

Gu, B., Mehlhorn, T.L., Liang, L., McCarthy, J.F., 1996. Competitive adsorption, displacement, and transport of organic matter on iron oxide: II. Displacement and transport. Geochim. Cosmochim. Acta 60, 2977–2992. doi:10.1016/0016-7037(96)00157-3

Gu, B., Schmitt, J., Chen, Z., Liang, L., McCarthy, J.F., 1995. Adsorption and desorption of different organic matter fractions on iron oxide. Geochim. Cosmochim. Acta 59, 219–229. doi:10.1016/0016-7037(94)00282-Q

Han, J., Kim, M., Ro, H.M., 2020. Factors modifying the structural configuration of oxyanions and organic acids adsorbed on iron (hydr)oxides in soils. A review, Environmental Chemistry Letters. Springer International Publishing. doi:10.1007/s10311-020-00964-4

Han, M., Lawler, D.F., 1992. The (Relative) Insignificance of G in Flocculation. J. Am. Water Works Assoc. 84, 79–91. doi:10.1002/j.1551-8833.1992.tb05869.x

Hotze, E.M., Phenrat, T., Lowry, G. V, 2010. Nanoparticle Aggregation: Challenges to Understanding Transport and Reactivity in the Environment. J. Environ. Qual. 39, 1909–

1924. doi:10.2134/jeq2009.0462

IHSS, 2020. Acidic Functional Groups of IHSS Samples [WWW Document]. URL http://humic-substances.org/acidic-functional-groups-of-ihss-samples/ (accessed 2.12.20).

Ittekkot, V., Laane, R.W.P.M., 1991. Fate of riverine particulate organic matter. SCOPE 42 - Biogeochem. Major World Rivers 233–243.

Konan, K.L., Peyratout, C., Bonnet, J.-P., Smith, A., Jacquet, A., Magnoux, P., Ayrault, P., 2007. Surface properties of kaolin and illite suspensions in concentrated calcium hydroxide medium. J. Colloid Interface Sci. 307, 101–108. doi:10.1016/j.jcis.2006.10.085

Kosmulski, M., 2014. The pH dependent surface charging and points of zero charge. VI. Update. J. Colloid Interface Sci. 426, 209–212. doi:10.1016/j.jcis.2014.02.036

Kosmulski, M., 2001. Chemical properties of material surfaces. Marcel Dekker, New York.

Kunhi Mouvenchery, Y., Kučerík, J., Diehl, D., Schaumann, G.E., 2012. Cation-mediated cross-linking in natural organic matter: a review. Rev. Environ. Sci. Bio/Technology 11, 41–54. doi:10.1007/s11157-011-9258-3

Lee, B., Hur, J., Toorman, E., 2017. Seasonal Variation in Flocculation Potential of River Water: Roles of the Organic Matter Pool. Water 9, 335. doi:10.3390/w9050335

Lee, B.J., Kim, J., Hur, J., Choi, I.H., Toorman, E.A., Fettweis, M., Choi, J.W., 2019. Seasonal Dynamics of Organic Matter Composition and Its Effects on Suspended Sediment Flocculation in River Water. Water Resour. Res. 55, 6968–6985. doi:10.1029/2018WR024486

Mannino, A., Harvey, H.R., 2000. Biochemical composition of particles and dissolved organic matter along an estuarine gradient: Sources and implications for DOM reactivity. Limnol. Oceanogr. 45, 775–788. doi:10.4319/lo.2000.45.4.0775

Meier, M., Namjesnik-Dejanovic, K., Maurice, P.A., Chin, Y.-P., Aiken, G.R., 1999. Fractionation of aquatic natural organic matter upon sorption to goethite and kaolinite. Chem. Geol. 157, 275–284. doi:10.1016/S0009-2541(99)00006-6

Morris, G., Harding, S., 2009. Polysaccharides, Microbial, in: Encyclopedia of Microbiology. Elsevier, pp. 482–494. doi:10.1016/B978-012373944-5.00135-8

Newcomb, C.J., Qafoku, N.P., Grate, J.W., Bailey, V.L., De Yoreo, J.J., 2017. Developing a molecular picture of soil organic matter–mineral interactions by quantifying organo–mineral binding. Nat. Commun. 8, 396. doi:10.1038/s41467-017-00407-9

Novich, B.E., Ring, T.A., 1985. Photon correlation spectroscopy of a coagulating suspension of illite platelets. J. Chem. Soc. Faraday Trans. 1 Phys. Chem. Condens. Phases 81, 1455. doi:10.1039/f19858101455

OECD, 2017. Test No. 318: Dispersion Stability of Nanomaterials in Simulated Environmental Media, OECD Guidelines for the Testing of Chemicals, Section 3. OECD, Paris.

doi:10.1787/9789264284142-en

Pecini, E.M., Avena, M.J., 2013. Measuring the Isoelectric Point of the Edges of Clay Mineral Particles: The Case of Montmorillonite. Langmuir 29, 14926–14934. doi:10.1021/la403384g

Peijnenburg, W.J.G.M., Baalousha, M., Chen, J., Chaudry, Q., Von Der Kammer, F., Kuhlbusch, T. a. J., Lead, J., Nickel, C., Quik, J.T.K., Renker, M., Wang, Z., Koelmans, A. a., 2015. A review of the properties and processes determining the fate of engineered nanomaterials in the aquatic environment. Crit. Rev. Environ. Sci. Technol. 3389, 00–00. doi:10.1080/10643389.2015.1010430

Petosa, A.R., Jaisi, D.P., Quevedo, I.R., Elimelech, M., Tufenkji, N., 2010. Aggregation and Deposition of Engineered Nanomaterials in Aquatic Environments: Role of Physicochemical Interactions. Environ. Sci. Technol. 44, 6532–6549. doi:10.1021/es100598h

Philippe, A., Schaumann, G.E., 2014. Interactions of Dissolved Organic Matter with Natural and Engineered Inorganic Colloids: A Review. Environ. Sci. Technol. 48, 8946–8962. doi:10.1021/es502342r

Poulton, S.W., Raiswell, R., 2005. Chemical and physical characteristics of iron oxides in riverine and glacial meltwater sediments. Chem. Geol. 218, 203–221. doi:10.1016/j.chemgeo.2005.01.007

Praetorius, A., Arvidsson, R., Molander, S., Scheringer, M., 2013. Facing complexity through informed simplifications: a research agenda for aquatic exposure assessment of nanoparticles. Environ. Sci. Process. Impacts 15, 161–168. doi:10.1039/c2em30677h

Praetorius, A., Badetti, E., Brunelli, A., Clavier, A., Gallego-Urrea, J.A., Gondikas, A., Hassellöv, M., Hofmann, T., Mackevica, A., Marcomini, A., Peijnenburg, W., Quik, J.T.K., Seijo, M., Stoll, S., Tepe, N., Walch, H., von der Kammer, F., 2020. Strategies for determining heteroaggregation attachment efficiencies of engineered nanoparticles in aquatic environments. Environ. Sci. Nano 7, 351–367. doi:10.1039/C9EN01016E

Preocanin, T., Abdelmonem, A., Montavon, G., Luetzenkirchen, J., 2016. Charging Behavior of Clays and Clay Minerals in Aqueous Electrolyte Solutions — Experimental Methods for Measuring the Charge and Interpreting the Results, in: Clays, Clay Minerals and Ceramic Materials Based on Clay Minerals. InTech, pp. 137–144. doi:10.5772/62082

Ratpukdi, T., Rice, J.A., Chilom, G., Bezbaruah, A., Khan, E., 2009. Rapid Fractionation of Natural Organic Matter in Water Using a Novel Solid-Phase Extraction Technique. Water Environ. Res. 81, 2299–2308. doi:10.2175/106143009X407302

Salminen, R., Batista, M.J., Bidovec, M., Demetriades, A., De Vivo, B., De Vos, W., Duris, M., Gilucis, A., Gregorauskiene, V., Halamic, J., Heitzmann, P., Lima, A., Jordan, G., Klaver, G., Klein, P., Lis, J., Locutura, J., Marsina, K., Mazreku, A., O'Connor, P.J., Olsson, S.Å., Ottesen, R.-T., Petersell, V., Plant, J.A., Reeder, S., Salpeteur, I., Sandström, H., Siewers, U., Steenfelt, A., Tarvainen, T., 2005. Geochemical Atlas of Europe. Part 1: Background Information, Methodology and Maps. Geological Survey of Finland, Espoo.

Schumacher, M., Christl, I., Vogt, R.D., Barmettler, K., Jacobsen, C., Kretzschmar, R., 2006. Chemical composition of aquatic dissolved organic matter in five boreal forest catchments sampled in spring and fall seasons. Biogeochemistry 80, 263–275. doi:10.1007/s10533-006-9022-x

Séquaris, J.-M., 2010. Modeling the effects of Ca2+ and clay-associated organic carbon on the stability of colloids from topsoils. J. Colloid Interface Sci. 343, 408–414. doi:10.1016/j.jcis.2009.12.014

Shao, H., Chang, J., Lu, Z., Grundy, J.S., Xie, G., Xu, Z., Liu, Q., 2020. Probing Interaction of Divalent Cations with Illite Basal Surfaces by Atomic Force Microscopy. J. Phys. Chem. C 124, 2079–2087. doi:10.1021/acs.jpcc.9b11202

Sharma, V.K., Ma, X., Guo, B., Zhang, K., 2021. Environmental factors-mediated behavior of microplastics and nanoplastics in water: A review. Chemosphere 271, 129597. doi:10.1016/j.chemosphere.2021.129597

Shrimali, K., Jin, J., Hassas, B.V., Wang, X., Miller, J.D., 2016. The surface state of hematite and its wetting characteristics. J. Colloid Interface Sci. 477, 16–24. doi:10.1016/j.jcis.2016.05.030

Tarasevich, Y.I., Polyakova, I.G., Polyakov, V.E., 2002. Hydrophilicity–Hydrophobicity Characteristics of Solid Surfaces and the State of Water near Surfaces of a Various Nature. Adsorpt. Sci. Technol. 20, 927–935. doi:10.1260/02636170260555831

Thill, A., Lambert, S., Moustier, S., Ginestet, P., Audic, J.M., Bottero, J.Y., 2000. Structural Interpretations of Static Light Scattering Patterns of Fractal Aggregates. J. Colloid Interface Sci. 228, 386–392. doi:10.1006/jcis.2000.6836

Tombácz, E., Libor, Z., Illés, E., Majzik, A., Klumpp, E., 2004. The role of reactive surface sites and complexation by humic acids in the interaction of clay mineral and iron oxide particles. Org. Geochem. 35, 257–267. doi:10.1016/j.orggeochem.2003.11.002

Tombs, M.P., Harding, S.E., 1997. An Introduction to Polysaccharide Biotechnology, An Introduction to Polysaccharide Biotechnology. CRC Press. doi:10.4324/9780203483411

Vázquez-Ortega, A., Hernandez-Ruiz, S., Amistadi, M.K., Rasmussen, C., Chorover, J., 2014. Fractionation of Dissolved Organic Matter by (Oxy)Hydroxide-Coated Sands: Competitive Sorbate Displacement during Reactive Transport. Vadose Zo. J. 13, 1–13. doi:10.2136/vzj2013.10.0179

Vindedahl, A.M., Strehlau, J.H., Arnold, W.A., Penn, R.L., 2016. Organic matter and iron oxide nanoparticles: aggregation, interactions, and reactivity. Environ. Sci. Nano 3, 494–505. doi:10.1039/C5EN00215J

Walch, H., von der Kammer, F., Hofmann, T., 2022. Freshwater suspended particulate matter—Key components and processes in floc formation and dynamics. Water Res. 220, 118655. doi:10.1016/j.watres.2022.118655

Walsch, J., Dultz, S., 2010. Effects of pH, Ca- and SO 4 -concentration on surface charge and

colloidal stability of goethite and hematite – consequences for the adsorption of anionic organic substances. Clay Miner. 45, 1–13. doi:10.1180/claymin.2010.045.1.01

Wang, H., Adeleye, A.S., Huang, Y., Li, F., Keller, A.A., 2015. Heteroaggregation of nanoparticles with biocolloids and geocolloids. Adv. Colloid Interface Sci. 226, 24–36. doi:10.1016/j.cis.2015.07.002

Wang, Hao, Zhao, X., Han, X., Tang, Z., Liu, S., Guo, W., Deng, C., Guo, Q., Wang, Huanhua, Wu, F., Meng, X., Giesy, J.P., 2017. Effects of monovalent and divalent metal cations on the aggregation and suspension of Fe3O4 magnetic nanoparticles in aqueous solution. Sci. Total Environ. 586, 817–826. doi:10.1016/j.scitotenv.2017.02.060

Wang, J., Zhao, X., Wu, F., Tang, Z., Zhao, T., Niu, L., Fang, M., Wang, H., Wang, F., 2021. Impact of montmorillonite clay on the homo- and heteroaggregation of titanium dioxide nanoparticles (nTiO2) in synthetic and natural waters. Sci. Total Environ. 784, 147019. doi:10.1016/j.scitotenv.2021.147019

Wang, W., Howe, J.Y., Gu, B., 2008. Structure and Morphology Evolution of Hematite (α-Fe 2 O 3) Nanoparticles in Forced Hydrolysis of Ferric Chloride. J. Phys. Chem. C 112, 9203–9208. doi:10.1021/jp800683j

Wang, X., Bolan, N., Tsang, D.C.W., Sarkar, B., Bradney, L., Li, Y., 2021. A review of microplastics aggregation in aquatic environment: Influence factors, analytical methods, and environmental implications. J. Hazard. Mater. 402, 123496. doi:10.1016/j.jhazmat.2020.123496

Yin, X., 2012. Anisotropic surface features of selected phyllosilicates. University of Utah.

Yu, S., Liu, J., Yin, Y., Shen, M., 2018. Interactions between engineered nanoparticles and dissolved organic matter: A review on mechanisms and environmental effects. J. Environ. Sci. 63, 198–217. doi:10.1016/j.jes.2017.06.021